PONTIFICIA UNIVERSIDAD CATOLICA DE CHILE
FACULTAD DE FISICA
INSTITUTO DE FISICA

A 1D TOPOLOGICAL INSULATOR FOR LIGHT

by

Daniel Esteban Pérez Tobar

Thesis submitted to the Faculty of Physics
of Pontificia Universidad Católica de Chile, as one of the requirements
to qualify for the academic Master's degree in Physics.

Supervisor	:	Dr. Sebastián Reyes (PUC Chile)
Committee	:	Dr. Giuseppe De Nittis (PUC Chile)
Committee	:	Dr. Roberto Rodríguez (PUC Chile)

December, 2020
Santiago, Chile

I guess this is as far as we go

Acknowledgements

Este trabajo, que no fue fácil de realizar fue posible gracias al apoyo de muchas personas que no puedo dejar de mencionar.

En primer lugar quisiera comenzar agradeciendo a, mi profesor, Sebastián Reyes. A pesar de las circunstancias externas que tuvimos que sortear durante este proceso, lo que aprendí de él y con él es algo que sé que llevaré conmigo a futuro.

En segundo lugar quisiera agradecer a los miembros de mi comisión revisora. Al profesor Giuseppe De Nittis, quien fue quien nos introdujo a este interesante tema y cuya disposición para aclarar dudas no puedo dejar de mencionar. Al profesor Roberto Rodríguez, cuya disposición y su retroalimentación acerca del trabajo presentado fueron una parte importante de que haya resultado.

También quisiera agradecer a mi familia y amigos. Su compañía y apoyo fueron fundamentales en los momentos difíciles. Sabrán quienes son.

Quiero agradecerle a IDLES porque con su música hicieron que aprendiera cosas de mí que no había visto y que me ayudaron a crecer y a sentirme bien conmigo mismo.

Quiero agradecer también a Antonia Orellana. Sus ganas de hacer de este país uno mejor me motivaron a trabajar más duro para poder terminar este trabajo.

A la cerveza, por mantener mi mente fresca. Al vino, por abrigarme cuando tenía frío. A la piscola, por mantenerme jovial.

Finalmente, agradecer al tío del marido de Pampita. Su lucha contra el Covid fue un ejemplo de superación que me motivó a salir adelante, cuando la cosa estaba más compleja.

Abstract

A 1D photonic topological insulator is the photonic realization of a 1D topological insulator. We show how the calculation of a topological invariant, known as the Zak phase, is a useful tool to identify different topologies in one-dimensional systems. We found topological phase transitions for the 1D photonic topological insulator and its relation to the inversion symmetry of the system.

Contents

Chapter 1

Introduction

As the title says, this is a work about Photonic Topological Insulators in one dimension and, thus, it is useful to get a general idea about what they are. First, we should ask, what is an insulator? In solid-state physics, we usually classify crystalline materials as conductors, semiconductors, and insulators, depending on their band structure and Fermi level. Insulators present an energy gap between the valence and the conduction band, which contains the Fermi level and, therefore, it is necessary a large amount of energy, compared to a semiconductor, to remove an electron from the valence band into the conduction band. Therefore, an insulator will not exhibit an electrical current in the presence of an electrical field. Second, we should refer to the word topological. Topology is a mathematical subject that deals with the preservation of properties of a geometrical object after being transformed continuously. And therefore, two objects are topologically equivalent if they can be continuously deformed one into the other. Topology is a relevant concept because two objects with different topologies will show different properties, such as conductivity, for example. Therefore, a topological insulator will present features that do not exist in standard (non-topological) insulators. Finally, we should clarify what we mean by the word photonic. A regular crystal, in the solid-state physics context, is made by atoms bounded, forming a periodic potential for the electrons within it. Instead, a photonic crystal is a structure constructed with materials whose dielectric function is periodic for the electromagnetic waves. Therefore, a photonic topological insulator is a photonic structure

that shows an unusual insulating properties for the electromagnetic waves in it, described by the mathematical tools of topology, in one direction.

1.1 About This Work

The previous description describes, conceptually, what we are studying in this thesis. The central idea is to set the main topics that we are revisiting in this work, Photonic Topological Insulators in one dimension.

In chapter 2, we will review topological concepts and the Quantum Hall Effect. This effect is the starting point to understand what topological insulators are. And then, the Su-Schrieffer-Heeger (SSH) model for polyacetylene, the most known one-dimensional topological insulator. This model is relevant as there are some physical effects in one dimension which are not exactly as in higher dimensions.

In chapter 3, we will discuss Photonic Crystals and their mathematical description, beginning with Maxwell's equations and their physical properties. Then, going to show the model that we studied. Finally, we are going to see, in a detailed form, the topological phase transitions for our model.

Finally, in chapter 4, we are going to give our main conclusions about the model studied, and open a brief discussion about future theoretical work and possible applications and experimental realization.

Chapter 2

Topology in Solid State Physics

"Topology can be thought of as a kind of generalization of Euclidean geometry, and also a natural framework for the study of continuity" [1].

2.1 Topology

The concept of topology can be understood as the mathematical field that deals with shapes and their classification. The most common example of two topologically distinct objects is the difference between a sphere and a torus. The topological difference between these two objects relies on the existence of a hole in the torus. It is not possible to continuously transform a sphere into a torus as we would have to break it by adding a hole. On the other hand, it is possible to notice that a sphere is topologically equivalent to a glass as the torus is to a cup.

To close or to open a hole is a problem because it implies a non-continuous transformation. We mentioned how the glass is topologically equivalent to a sphere as we can transform continuously one into another and, we can do the same for the coffee cup-torus. Two objects, or systems, will be said to be **homeomorphic** if it is possible to transform continuously one into another.

As an example, we can see that an open disc $D^2 = (x, y) \in \mathbb{R}^2 | x^2 + y^2| < 1$ is homeo-

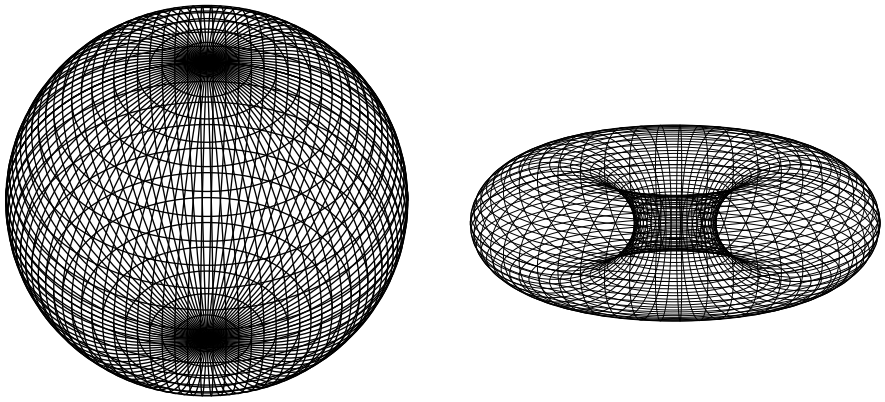

(a) (b)

Figure 2.1: The sphere in (a) and the torus in (b) can be distinguished topologically for their number of holes.

morphic to $\mathbb{R}^2$ and a **homeomorphism** $f : D^2 \longrightarrow \mathbb{R}^2$ may be

$$f(x,y) = \left(\frac{x}{\sqrt{1-x^2-y^2}}, \frac{y}{\sqrt{1-x^2-y^2}} \right), \tag{2.1}$$

whose inverse $f^{-1} : \mathbb{R}^2 \longrightarrow D^2$ is

$$f(x,y) = \left(\frac{x}{\sqrt{1+x^2+y^2}}, \frac{y}{\sqrt{1+x^2+y^2}} \right), \tag{2.2}$$

Where we note that f is a continuous map and, it is easy to check that $f^{-1}\left(f(x,y)\right) = (x,y)$.

To distinguish, topologically, two objects it is necessary to introduce the concept of **topological invariant**. These are quantities that are preserved under homeomorphisms and are useful because two objects with, at least, one different topological invariant will not be homeomorphic. Therefore, two objects with one or more different topological invariants, will not be topologically equivalent.

We can see, from the sphere-glass-torus-coffee cup example, that the *genus* (number of holes) is a topological invariant. Another accessible example, for a topological invariant, is the **Euler Characteristic**, defined as $\chi = V - E + F$, with V being the number of

vertices, E the number of edges and F the number of faces of a geometric figure.

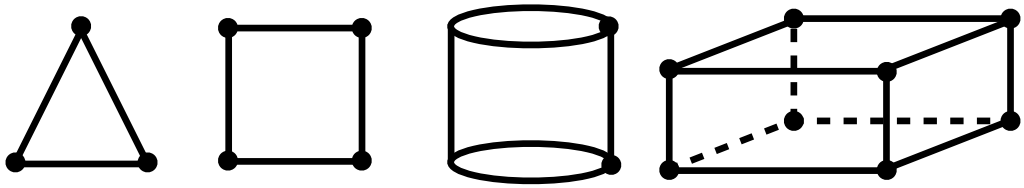

Figure 2.2: A triangle, an square, a cylinder and parallelepiped.

If we take the objects in Figure 2.2, we can see that the Euler characteristic for the triangle and the square is $\chi = 1$ and, for the cylinder and parallelepiped, is $\chi = 2$. Therefore, we know that the two first objects are different from the two others, topologically speaking. However, we can not assure that the triangle and the square are topologically equivalent. The topological invariant will only confirm if two objects are different from each other or will not give any information.

We will see that there are some physical quantities which are, in fact, topological invariants and will be useful to learn information about the physical system we are studying. One example of that is the Berry phase, which we will discuss in the next section. This phase will give us information about the degeneracies of the spectrum of an operator.

2.2 The Geometric Phase and The Berry Phase

A system that begins in a state $|\psi\rangle$ if evolved adiabatically, in some parameter space, will acquire a dynamical phase factor and a geometrical phase factor[2, 3]. This is known as the quantum adiabatic theorem, shown in detail in Appendix A. Let us suppose we have a Hamiltonian $\hat{H}(\mathbf{R})$, which depends on a parameter set $\mathbf{R} = (X, Y, ...)$, in this case, time-dependent with a periodicity T, $\mathbf{R}(t + T) = \mathbf{R}(t)$. The evolution, in time, of that state $|\psi\rangle$ is described by the time-dependent Schrödinger equation

$$\hat{H}(\mathbf{R}(t))\,|\psi(t)\rangle = i\hbar\,|\dot{\psi}(t)\rangle\,. \tag{2.3}$$

At any time t, for the natural basis of discrete eigenstates $|n(\mathbf{R}(t))\rangle$ of $\hat{H}(\mathbf{R}(t))$ we

have the condition

$$\hat{H}(\mathbf{R}(t))\,|n(\mathbf{R}(t))\rangle = E_n(\mathbf{R}(t))\,|n(\mathbf{R}(t))\rangle\,. \tag{2.4}$$

Naturally, the phase of the eigenstate $|n(\mathbf{R}(t))\rangle$ is not relevant for this equation, as will be a global phase in both sides of the equation, thus is ignored.

A system prepared initially in the state $|n(\mathbf{R}(0))\rangle$, evolving adiabatically with $\hat{H}$, will be $|n(\mathbf{R}(t))\rangle$ at the time t. Then, the state $|\psi\rangle$ at that time t can be expressed as

$$|\psi(t)\rangle = \exp\left(-\frac{i}{\hbar}\int_0^t E_n(\mathbf{R}(t'))dt'\right)\exp\left(i\gamma_n(t)\right)|n(\mathbf{R}(t))\rangle\,, \tag{2.5}$$

where the first phase factor is known as the *dynamical phase*, and the second one is the *geometric phase*. We are concentrating on the geometric phase, as it is the one that will give the relevant information we mentioned before.

First, we have to note that this phase is non-integrable and can not be written as a function of $\mathbf{R}$ and if we evolve the system on a full circuit, $(0 \to T)$, it is not single-valued, $\gamma_n(0) \neq \gamma_n(T)$.

To get an explicit expression for the geometric phase, we use the definition in Eq. (2.5) for the time-dependent Schrödinger equation, and get a differential equation

$$\dot{\gamma}_n(t) = i\,\langle n(\mathbf{R}(t))|\nabla_{\mathbf{R}} n(\mathbf{R}(t))\rangle \cdot \dot{\mathbf{R}}(t), \tag{2.6}$$

and for the evolution round a circuit $\mathcal{C}$ we obtain,

$$\gamma_n(\mathcal{C}) = i\oint_{\mathcal{C}} \langle n(\mathbf{R}(t))|\nabla_{\mathbf{R}} n(\mathbf{R}(t))\rangle \cdot d\mathbf{R}, \tag{2.7}$$

where the line integral is closed as we are going over a cycle.

The Berry phase is be defined as

$$\gamma_n(\mathcal{C}) = \oint_{\mathcal{C}} \mathcal{A}(\mathbf{R}) \cdot d\mathbf{R}, \tag{2.8}$$

where

$$\mathcal{A}(\mathbf{R}) = i\,\langle n(\mathbf{R}(t))|\nabla_{\mathbf{R}} n(\mathbf{R}(t))\rangle \tag{2.9}$$

is called the *Berry connection*.

As the Berry phase is defined as a line integral, over a simple closed-loop, it is possible to use the Stoke's theorem to get another expression for it. This is,

$$\gamma_n(\mathcal{C}) = -\iint_{S_\mathcal{C}} d\mathbf{S} \cdot \mathbf{V}_n(\mathbf{R}), \tag{2.10}$$

where

$$\mathbf{V}_n(\mathbf{R}) = \Im \sum_{n \neq m} \frac{\langle n(\mathbf{R}) | \nabla_\mathbf{R} \hat{H}(\mathbf{R}) | m(\mathbf{R}) \rangle \times \langle m(\mathbf{R}) | \nabla_\mathbf{R} \hat{H}(\mathbf{R}) | n(\mathbf{R}) \rangle}{(E_m(\mathbf{R}) - E_n(\mathbf{R}))^2}. \tag{2.11}$$

$\Im$ denotes the imaginary part. This quantity is known as the Berry curvature and is obtained as the curl of the Berry connection. It is very convenient to remark that, for this expression, we have no dependence on $|\nabla_\mathbf{R} n(\mathbf{R})\rangle$, thus any solution of Equation 2.4 can be used to calculate $\mathbf{V}_n(\mathbf{R})$ and, as it is the curl of a function, its divergence is zero. Therefore, this result does not depend on the chosen integration surface.

It is necessary to remark, as an important feature, that the Berry phase is not gauge-dependent (see Appendix B for more details).

To understand more about the utility of the Berry phase, we can revisit the example provided by Berry. Let us take a Hamiltonian given by $\hat{H}(\mathbf{R}) = \frac{1}{2}\mathbf{R} \cdot \hat{\sigma}$, which is a two-level system, where $\mathbf{R} = (X, Y, Z)$ and $\hat{\sigma}$ is the vector of Pauli matrices. Thus the Hamiltonian, for this system, is

$$\hat{H}(\mathbf{R}) = \frac{1}{2} \begin{bmatrix} Z & X - iY \\ X + iY & -Z \end{bmatrix}, \tag{2.12}$$

and its eigenvalues are

$$E_\pm(\mathbf{R}) = \pm \frac{1}{2} \sqrt{X^2 + Y^2 + Z^2}. \tag{2.13}$$

It is easy to see from (2.13) that there is a degeneracy point at $\mathbf{R} = 0$. But we would like to prove that the Berry phase can be used to deduce this.

Let us call the eigenstates of this two-level system as $|+\rangle$ and $|-\rangle$, according to the sign

of the eigenvalues $E_+(\mathbf{R})$ and $E_-(\mathbf{R})$. Then the Berry phase for this two-level system is

$$\gamma_\pm(C) = i \oint_C \langle \pm | \nabla_{\mathbf{R}} \pm \rangle \cdot d\mathbf{R}. \tag{2.14}$$

Using Stoke's theorem, we can rewrite the line integral as a surface integral. Therefore, the Berry phase is expressed as

$$\gamma_\pm(C) = \iint_{S_C} \nabla \times i \langle \pm | \nabla_{\mathbf{R}} \pm \rangle \cdot d\mathbf{S}, \tag{2.15}$$

and after some calculations, it is possible to rewrite it as

$$\gamma_\pm(C) = \mp \iint_{S_C} \frac{\mathbf{R}}{2R^3} \cdot d\mathbf{S}. \tag{2.16}$$

Michael Berry proved that this phase change, $\gamma_\pm(C)$ is the *"flux through C of the magnetic field of a monopole with strength $-\frac{1}{2}$ located at the degeneracy"*. Then the Berry phase corresponding to the curve C is

$$e^{i\gamma_\pm(C)} = e^{\mp \frac{1}{2} i\Omega(C)}, \tag{2.17}$$

with $\Omega(C)$ the solid angle that C subtends at the singular point $\mathbf{R} = 0$. This result is *"independent of the choice of the surface spanning C, because Ω can change only in multiples of 4π"*.

For the particular case $Y = 0$, any curve C belongs on the plane XZ and $E_+(\mathbf{R})$ and $E_-(\mathbf{R})$ intersect conically at the degeneracy point at $\mathbf{R} = 0$. In this case, only two possible outcomes are possible, depending on the curve C enclosing the degeneracy point or not. Therefore, the Berry phase is

$$e^{i\gamma_\pm(C)} = \begin{cases} -1, \text{if } C \text{ encircles the degeneracy,} \\ 1, \text{otherwise.} \end{cases} \tag{2.18}$$

This example can be considered too simple as it is easy to see, from the spectrum, that there is a degeneration for $\mathbf{R} = 0$. However, it set the foundations to understand how we

can use the Berry phase to obtain information about a physical system. As we are working with solid-state systems, we would like to show how to calculate the Berry phase within this context. Therefore, before we get into those details, we are going to revisit the theory of Band Structure and Bloch's theorem.

2.3 Band Structure and Bloch's Theorem

In solid-state physics, a crystal is described by the lattice vectors $\mathbf{R}$, which are defined as linear combinations of the primitive lattice vectors $\mathbf{a}_i$,

$$\mathbf{R} = \sum_{i=1}^{D} n_i \mathbf{a}_i, \tag{2.19}$$

where the coefficients n_i are integers and, D is the crystal's dimension. It is necessary to state also, the primitive unit cell's (PUC) definition. The PUC is the basic unit, the fundamental building block, of a crystal as we will construct one by moving it using all the lattice vectors, without generation of voids or overlaps. However, although we use the primitive lattice vectors to define the PUC, there are other definitions for it. An alternative definition for the PUC is the Wigner-Seitz cell, which is defined as *the locus of points in space that are closer to that lattice point than any other lattice points.*

Even though we have the description of a crystal in real space, most of the analysis in solid-state physics is done at the reciprocal lattice, which is the inverse space of the real space lattice [4]. Thus, we define the reciprocal lattice vector, $\mathbf{K}$, as

$$\mathbf{K} = \sum_{i=1}^{D} m_i \mathbf{b}_i, \tag{2.20}$$

where the coefficients m_i are, again, integers and D is the crystal's dimension. We can also define a PUC for the reciprocal space but, if we use the same definition of the Wigner-Seitz cell in this space, we will get the **Brillouin Zone**.

The relation between the real space and the reciprocal space is given by the primitive

lattice vectors and the primitive reciprocal lattice vectors,

$$\mathbf{a}_i \cdot \mathbf{b}_j = 2\pi\delta_{ij}. \tag{2.21}$$

It is easy to see, from Equation 2.21, that $\mathbf{R} \cdot \mathbf{K} = 2\pi l$, where l is an integer equals to the sum of $n_i m_i$.

Any function with the same periodicity as the lattice can be written in the form

$$f(\mathbf{r}) = \sum_{\mathbf{K}} e^{i\mathbf{K}\cdot\mathbf{r}} f(\mathbf{K}), \tag{2.22}$$

where $f(\mathbf{K})$ are the components of the Fourier transform. Therefore, for any given function with the same periodicity of the crystal, we will focus only on $\mathbf{r}$ within the PUC, this is known as Bloch's theorem.

For a potential with the same translational symmetry as the lattice, $V(\mathbf{R}+\mathbf{r}) = V(\mathbf{r})$, the single-particle wavefunctions, which solves the Schrödinger equation for that potential, will have the same symmetry and, therefore, the Hamiltonian and the translation operator, in $\mathbf{R}$, will commute. That

$$\left[\hat{T}_{\mathbf{R}}, \hat{H}\right] = 0. \tag{2.23}$$

Therefore, as these two operators commute, the eigenfunctions for the given Hamiltonian are of the form

$$\psi_{\mathbf{k}}(\mathbf{r}+\mathbf{R}) = e^{i\mathbf{k}\cdot\mathbf{R}}\psi_{\mathbf{k}}(\mathbf{r}), \tag{2.24}$$

and we can rewrite these wavefunctions as

$$\psi_{\mathbf{k}}(\mathbf{r}) = e^{i\mathbf{k}\cdot\mathbf{r}}u_{\mathbf{k}}(\mathbf{r}), \tag{2.25}$$

where $u_{\mathbf{k}}(\mathbf{r})$ is periodic in $\mathbf{R}$.

Let us take the time-independent Schrödinger equation for a non-relativistic single particle,

$$\left[-\frac{\hbar^2}{2m}\nabla^2 + V(\mathbf{r})\right]\psi_{\mathbf{k}}(\mathbf{r}) = \epsilon_{\mathbf{k}}\psi_{\mathbf{k}}(\mathbf{r}). \tag{2.26}$$

Using the ansatz in Equation 2.25 for the time-independent Schrödinger equation, we will obtain the equation for $u_k()$,

$$\left[\frac{\hbar^2}{2m}(-i\nabla + \mathbf{k})^2 + V(\mathbf{r})\right] u_{\mathbf{k}}(\mathbf{r}) = \epsilon_{\mathbf{k}} u_{\mathbf{k}}(\mathbf{r}). \tag{2.27}$$

As it is possible to have more than one solution, for the same $\mathbf{k}$, within the Brillouin zone, it is necessary to introduce a new index to identify the single-particle solutions for Equation 2.27. Therefore, the wavefunctions which are solutions of the equation will be of the form $\psi_{n\mathbf{k}}(\mathbf{r})$, where n is a discrete, integer, index and it will indicate each one of the energy bands, given by $\epsilon_{n\mathbf{k}}$, which form the band structure of the system. An example of the band-structure of a crystalline system is depicted in Figure 2.3. The particular model to which it belongs will be discussed, with more detail, in section 2.6. One of the most relevant characteristics that we can learn from a crystal's band-structure, at least for our particular interest, is how to classify the system in terms of whether it is a conductor, a semiconductor or an insulator. This classification is made by looking at where the Fermi level is. If the Fermi level is in a non-filled band, the system is a conductor, but if it is within the energy gap, then it is a semiconductor or an insulator. The difference between those two is in the energy gap. For a semiconductor, the energy gap is around 1 eV of energy, but for an insulator, it is higher.

Our goal is to study topological insulators. These materials behave, on its trivial phase, as normal insulators. However, for non-trivial phases or **non-trivial topologies**, there will be unexpected features, *exotic states of matter*. To be able to understand what is trivial and a non-trivial topology and this novel physical features, related to the non-trivial topologies of a crystal, we are going to study, what can we learn from the Bloch bands, by calculating the Berry phase.

2.4 Berry Phase in Bloch Bands

As we already discussed, the Berry phase is obtained by the adiabatic evolution in some parameter space, over a closed path. As we are working with Bloch bands, it is natural to work within the $\mathbf{k} - space$, which can be taken as the parameter space $\mathbf{R}$ in the Berry

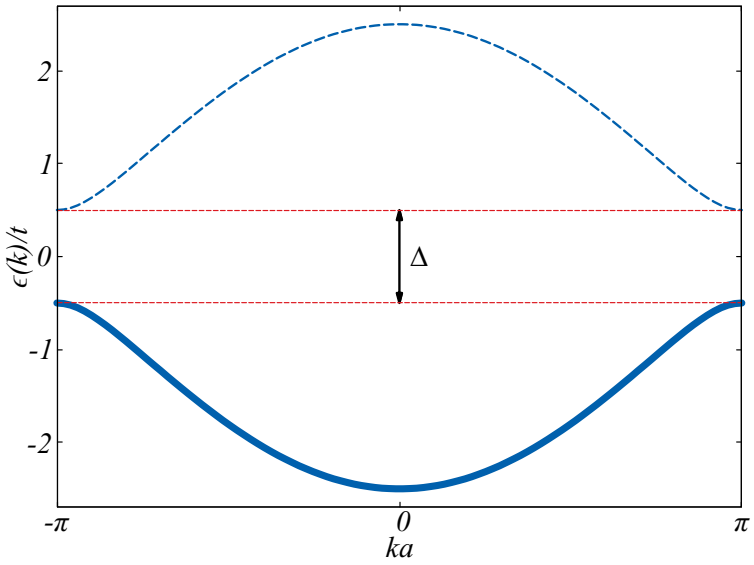

Figure 2.3: A two-band structure spectrum, for the SSH model, with a bandgap of $\Delta = 2\,eV$. The particular model is discussed in section 2.6.

example. Therefore, the Berry phase is written as

$$\gamma_n(\mathcal{C}) = i \oint_{\mathcal{C}} \langle u_{n\mathbf{k}} | \nabla_{\mathbf{k}} u_{n\mathbf{k}} \rangle \, d\mathbf{k}. \tag{2.28}$$

With this new expression, we can calculate the Berry phase within the solid-state physics context, for electrons, in periodic potentials. But the question we should answer is, what can we extract from the Berry phase calculation of one of these states? Probably the most representative physical phenomenon to answer this question is the *Hall conduction quantization in graphene*. But before we get into that phenomena, it is necessary to review the **quantum Hall effect** and other physical processes, as we are going to see that there are several related.

2.4.1 Adiabatic Transport

Let us consider a one-dimensional insulator whose Hamiltonian is evolved adiabatically in time, preserving the lattice's translational symmetry. As the system's eigenstates can be represented as Bloch functions, it is natural to work in the k-space, as we already discussed. In this case, the Hamiltonian depends on time and the wave-vector k. The evolution in

time of the wavefunction $|\psi_{nk}(t)\rangle$, up to first order, is given by

$$|\psi_{nk}(t)\rangle \propto |u_{nk}(t)\rangle - i\hbar \sum_{n\neq m} \frac{|u_{mk}(t)\rangle \langle u_{mk}(t)|\partial_t u_{nk}(t)\rangle}{E_{nk}(t) - E_{mk}(t)}. \tag{2.29}$$

As we are thinking about transport, we need to get the expectation value for the velocity operator, which is defined as

$$\hat{v}(k) = \frac{1}{\hbar}\frac{\partial \hat{H}(k)}{\partial k}, \tag{2.30}$$

and we obtain that for the state $|\psi_{nk}(t)\rangle$ it is

$$v_n(k) \simeq \frac{1}{\hbar}\frac{\partial E_{nk}(t)}{\partial k} - i\sum_{n\neq m}\left[\frac{\langle u_{nk}(t)|\,\partial_k \hat{H}(t,k)\,|u_{mk}(t)\rangle \langle u_{mk}(t)|\partial_t u_{nk}(t)\rangle}{E_{nk}(t) - E_{mk}(t)} - \text{c.c.}\right]. \tag{2.31}$$

Using the fact that $\langle u_{nk}(t)|\,\partial_k \hat{H}(t,k)\,|u_{mk}(t)\rangle = (E_{nk}(t) - E_{mk}(t))\,\langle \partial_k u_{nk}(t)|u_{mk}\rangle$ we get

$$v_n(k) = \frac{\partial E_n(k)}{\partial k} - \underbrace{i\left[\langle \partial_k u_{nk}(t)|\partial_t u_{nk}(t)\rangle - \langle \partial_t u_{nk}(t)|\partial_k u_{nk}(t)\rangle\right]}_{\Omega_n(t,k)}, \tag{2.32}$$

where $\Omega_n(t,k)$ is the Berry curvature. To get the total current in our one-dimensional insulator, we have to integrate over the Brillouin zone and add for all the n filled bands. The zeroth-order vanishes, as the Brillouin zone is periodic, thus the total current is given by

$$j = -\sum_n \int \frac{dk}{2\pi}\Omega_n(t,k). \tag{2.33}$$

If we are interested in the number of particles transported over the cycle, we have to integrate over it,

$$C_n = -\int_0^T dt \int \frac{dk}{2\pi}\Omega_n(t,k). \tag{2.34}$$

This quantity, which is the Berry phase over a torus[1], divided by 2π, known as the **first Chern number**, is the number of particles transported, over the cycle, for the nth band. As we can not have particles' halves being transported, it must be an integer. However, the fact that this quantity is quantized is not a trivial statement, and we will revisit it in

[1] As t and k are periodic, the $2D$ parameter space (t,k) is a torus, T^2.

the next subsection before we continue.

2.4.2 First Chern Number Quantization

Let us take a two-dimensional parameter space, (t, k), with both parameters being periodic, thus, a torus T^2. It is possible to cut open the torus and display it as a rectangle, defining the coordinates $x = t/T$ and $y = k/2\pi$, as shown in Figure 2.4.

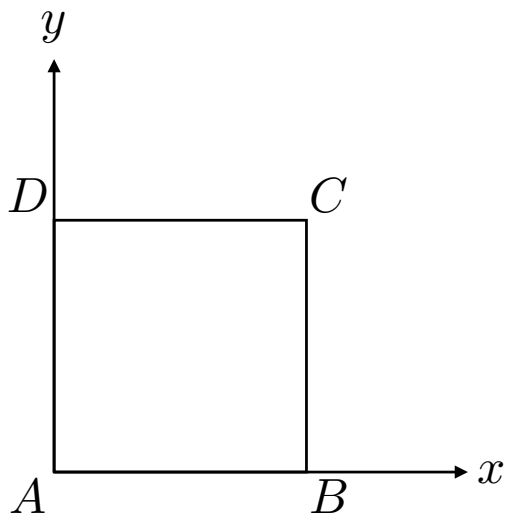

Figure 2.4: The two-dimensional open torus.

Using Stoke's theorem, it is possible to rewrite the integral in Equation 2.34 as a contour integral. This is

$$C = \frac{1}{2\pi}\left[\int_A^B \mathcal{A}_t(t,0)dt + \int_B^C \mathcal{A}_k(T,k)dk + \int_C^D \mathcal{A}_t(t,2\pi)dt + \int_D^A \mathcal{A}_k(0,k)dk\right], \quad (2.35)$$

where $\mathcal{A}_j(t,k) = \langle u(t,k)|\, i\nabla_j\, |u(t,k)\rangle$.

For each one of the integrals in Equation 2.35 we get a phase factor of the form $\exp(i\theta_j(j'))$. Thus, the first Chern number is

$$C = \frac{1}{2\pi}\left[\theta_t(T) - \theta_k(2\pi) + \theta_t(0) - \theta_k(0)\right]. \quad (2.36)$$

We need to keep in mind that, due to the periodic border conditions on the torus, $|u(t,0)\rangle$ and $|u(t,2\pi)\rangle$ are equal up to a phase, as for the other corners also. Therefore, we

get that

$$|u(0,0)\rangle = e^{i[\theta_t(T)-\theta_k(2\pi)+\theta_t(0)-\theta_k(0)]}\,|u(0,0)\rangle\,, \tag{2.37}$$

and as $|u\rangle$ is single-valued, the exponent has to be an integer multiple of 2π, and therefore, the first Chern number is an integer. If the torus has a degeneracy within it, the first Chern number will be non-zero, as we studied for the two-level system.

The quantization of the first Chern number, which we already have seen it is related to the adiabatic transport of electrons, which is directly related to the Quantum Hall effect. But before we get into it, we will discuss electron dynamics in the presence of electromagnetic fields.

2.4.3 Dynamics in a Electromagnetic Field

As we want to examine the Hall conductance quantization in graphene, we need to check the Quantum Hall Effect. But before we get into it, we need to check the electron's dynamics in the presence of an electromagnetic field, as it will evidence other properties of the Berry curvature.

Let us take an electron on a lattice described by the potential $V_L(\mathbf{r})$, moving in the presence of an electromagnetic field, which depends on time. The Hamiltonian describing the physics for that given electron is of the form

$$\hat{H}(t) = \frac{[\mathbf{p} + \frac{e}{c}\mathbf{A}]^2}{2m} + V_L(\mathbf{r}). \tag{2.38}$$

Considering the "Bloch problem", we can work within the k-space and introduce the gauge-invariant crystal momentum $\mathbf{k}'$ as

$$\mathbf{k}' = \mathbf{k} + \frac{e}{c\hbar}\mathbf{A}(t). \tag{2.39}$$

Using this new definition for the crystal momentum, we can label the system's eigenstates, just as we can do it with the usual $\mathbf{k}$. The new crystal momentum, $\mathbf{k}'$, satisfies the condition

$$\dot{\mathbf{k}'} = -\frac{e}{c\hbar}\mathbf{E}. \tag{2.40}$$

As we have changed the coordinates, if we want to calculate the velocity of an electron in the presence of an electromagnetic field, the derivatives are transformed, also, as

$$\frac{\partial}{\partial k_\alpha} \to \frac{\partial}{\partial k'_\alpha} \qquad \frac{\partial}{\partial t} \to -\left(\frac{e}{c\hbar}\right) E_\alpha \frac{\partial}{\partial k'_\alpha}, \tag{2.41}$$

thus, we get for the velocity

$$\mathbf{v}_n(\mathbf{k}') = \frac{\partial E_n(\mathbf{k}')}{\hbar \partial \mathbf{k}'} - \frac{e}{c\hbar}\mathbf{E} \times \mathbf{\Omega}_n(\mathbf{k}'), \tag{2.42}$$

where $\mathbf{\Omega}_n(\mathbf{k}')$ is, again, the Berry curvature.

The second term in Equation 2.42, known as *anomalous velocity*, leads to a current transverse to the electric field. Therefore, the description of the dynamics does not depend only on the usual band dispersion. The transverse current is what rises a Hall current, which is the one that we are interested in. The velocity formula should be invariant under time-reversal and spatial inversion operations for an unperturbed system with these symmetries [3]. Thus, for a time-reversal system, the Berry curvature satisfies $\mathbf{\Omega}_n(-\mathbf{k}) = -\mathbf{\Omega}_n(\mathbf{k})$ and for a system with spatial inversion symmetry $\mathbf{\Omega}_n(-\mathbf{k}) = \mathbf{\Omega}_n(\mathbf{k})$. Therefore, a system with both symmetries will have a zero Berry curvature. It means that we need to break, at least, one of these two symmetries to get a non-zero Berry curvature.

As we have seen in this section, the non-zero Berry curvature/phase is related to adiabatic transport and electron dynamics in materials. And one relevant physical phenomena where we can apply and get a better insight into the effects before mentioned is the Quantum Hall Effect.

2.5 The Quantum Hall Effect

Before getting into the details of the Quantum Hall Effect (QHE), it is useful to remember the classical Hall effect. This effect consists of the emergence of a voltage difference between two edges of a conductor, transverse to an electrical current in it, in the presence of a magnetic field, perpendicular to the given electrical current. If we consider a system like the one depicted in Figure 2.5, we would be able to measure a voltage difference be-

tween points a and b. This voltage difference, known as Hall voltage, and (subsequently) the Hall resistivity are both linear functions of the applied magnetic field.

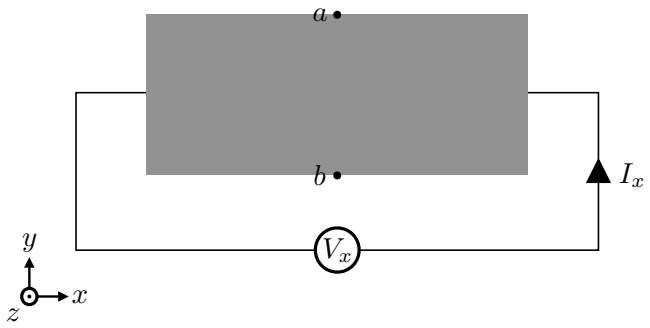

Figure 2.5: An schematic representation of a Hall Effect setting.

In 1980, when looking for a new method to measure the fine-structure constant, Klaus von Klitzing, Gerhard Dorda and Michael Pepper, discovered the QHE[2]. The novel feature of this effect was the fact that the Hall resistivity was no longer linear as a function of the applied magnetic field, but it developed steps. It was quantized. Their results are shown in Figure 2.6.

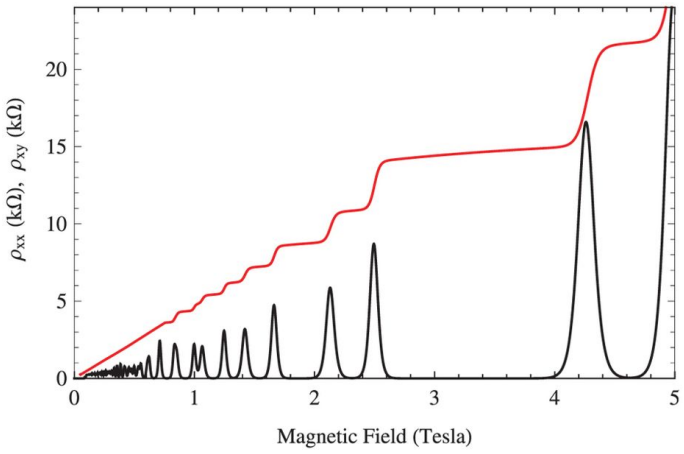

Figure 2.6: Results for the measure of the Hall resistivity (red line) and the longitudinal resistivity (black line) as a function of the magnetic field. *Sci. Rep.* **3**, 1075 (2013).

Now the question we have to answer is where does the quantization come? The Hall

[2]Nowadays, it is known as Integer Quantum Hall Effect.

conductivity can be obtained using the Nakano-Kubo formula. This is,

$$\sigma_{xy} = -ie^2\hbar \sum_{\epsilon_n<\epsilon_F<\epsilon_m} \frac{(v_y)_{nm}(v_x)_{mn} - (v_x)_{nm}(v_y)_{mn}}{(E_n - E_m)^2}, \tag{2.43}$$

where n and m label the energy bands below and above the Fermi energy (ϵ_F) and $(v_\alpha)_{nm}$ are the components of the velocity operator.

If we take into consideration what we have already discussed about adiabatic transport, we can note that it is possible to rewrite the conductivity as

$$\sigma_{xy}^{(n)} = \frac{-i}{2\pi}\frac{e^2}{h}\int d^2k \int d^2r \left(\frac{\partial u_{n\mathbf{k}}^*(x,y)}{\partial k_y}\frac{\partial u_{n\mathbf{k}}(x,y)}{\partial k_x} - \frac{\partial u_{n\mathbf{k}}^*(x,y)}{\partial k_x}\frac{\partial u_{n\mathbf{k}}(x,y)}{\partial k_y} \right), \tag{2.44}$$

which is the first Chern number in units of e^2/h [3]. This is,

$$\sigma_{xy}^{(n)} = \frac{e^2}{\hbar}\int_{BZ} \frac{d^2k}{(2\pi)^2}\Omega_n(\mathbf{k}). \tag{2.45}$$

Therefore, we can see that the Hall conductivity is strictly related to the Chern number and, obviously, to the Berry phase. We already saw that this quantity is quantized and, it is natural to question ourselves what are the physical consequences of this quantization. As we discussed before, it has some interesting implications in the transport of particles at the edges of the sample.

2.5.1 The Edge States

The emergence of edge states is one of the physical manifestations most interesting of the QHE and is strictly related to the conductance quantization. To get a better understanding of the emergence of these states, we are going to revisit the microscopic description of the QHE, as explained by Laughlin [5].

Let us consider a two-dimensional electron gas, confined in an infinite strip or a ribbon, as depicted in Figure 2.7. If we take a magnetic field, as mentioned previously, perpendicular to the sample as $\mathbf{A} = H_0 y\hat{x}$, in such a way that it is normal to the surface of the ribbon, the gauge transformation will multiply all localized states by a global phase factor

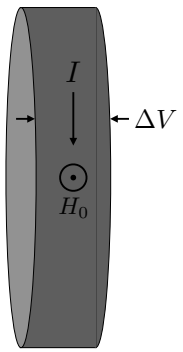

Figure 2.7: A metallic ribbon confining a 2D electron gas.

$\exp(ieAx/\hbar c)$ and will be possible only if

$$A = n\frac{hc}{eL}, \tag{2.46}$$

where n is an integer and L is the length of the ribbon. The Hamiltonian for this given system would be

$$H = \frac{1}{2m}\left(\mathbf{p} - \frac{e}{c}\mathbf{A}\right)^2 + eE_0 y, \tag{2.47}$$

where E_0 would is the electric field across the ribbon. The eigenfunctions for this Hamiltonian would be of the form

$$\psi_{n,k}(x,y) = e^{ikx}\phi_n(y - y_0), \tag{2.48}$$

where the function $\phi_n(y)$ are solutions of the Harmonic oscillator. This means it satisfies the equation

$$\frac{1}{2m}\left[p_y^2 + \left(\frac{eH_0}{c}\right)^2 y^2\right]\phi_n(y - y_0) = \hbar\omega_c\left(n + \frac{1}{2}\right)\phi_n(y - y_0), \tag{2.49}$$

where ω_c is the cyclotron frequency and $y_0 = \frac{1}{\omega_c}\left(\frac{\hbar k}{m} - \frac{cE_0}{H0}\right)$ is the position at where the functions ϕ_n are centered.

The center, y_0, of the function $\psi_n(y - y_0)$ is affected by a change in the vector potential

$\Delta A\hat{x}$ as

$$y_0 \quad \rightarrow \quad y_0 - \frac{\Delta A}{H_0}. \tag{2.50}$$

As the energy for this two-dimensional electron gas is given by

$$E_{nk} = \left(n + \frac{1}{2}\right)\hbar\omega_c + eE_0 y_0 + \frac{1}{2}m\left(\frac{cE_0}{H_0}\right), \tag{2.51}$$

the change in the center y_0 would shift the energy linearly.

We are now interested in the current of the system due to the potential difference ΔV between the edges. This current of the system can be defined by $c\Delta U/\Delta\phi$, where U is the total electronic energy and a change in a flux quantum, $\Delta\phi = hc/e$, would map the system into itself due to gauge invariance. Thus, the current which transfers n electrons from one edge into the other would be

$$I = c\frac{neV}{\Delta\phi} = n\frac{e^2}{h}V, \tag{2.52}$$

thus the conductance of the system is $G = ne^2/h$, which is the exact same result obtained by the Nakano-Kubo formula.

In Appendix D, we present a more in-depth discussion of the Laughlin pump, if needed.

The Berry phase quantization, the conductance quantization, and therefore, the emergence of a quantized current at the edges of the 2D electron gas is not a coincidence. The quantization of these quantities is a single phenomenon known as bulk-edge correspondence. The Berry phase is a bulk property and, the edge current is, obviously, an edge property. A non-zero Berry phase is related to a non-zero Hall conductance and the emergence of these edge states. The bulk will give us information about the edges and vice versa.

With the knowledge of these quantization and having in mind the concept of bulk-edge correspondence, we would like to study the Hall conductance quantization in a two-dimensional lattice, as is the case for graphene.

2.5.2 Hall Conductance Quantization in Graphene

Graphene is a two-dimensional material formed by carbon atoms in a honeycomb lattice, defined by the vectors $\mathbf{R}_1 = \frac{a}{2}(3, \sqrt{3})$ and $\mathbf{R}_2 = \frac{a}{2}(3, -\sqrt{3})$.

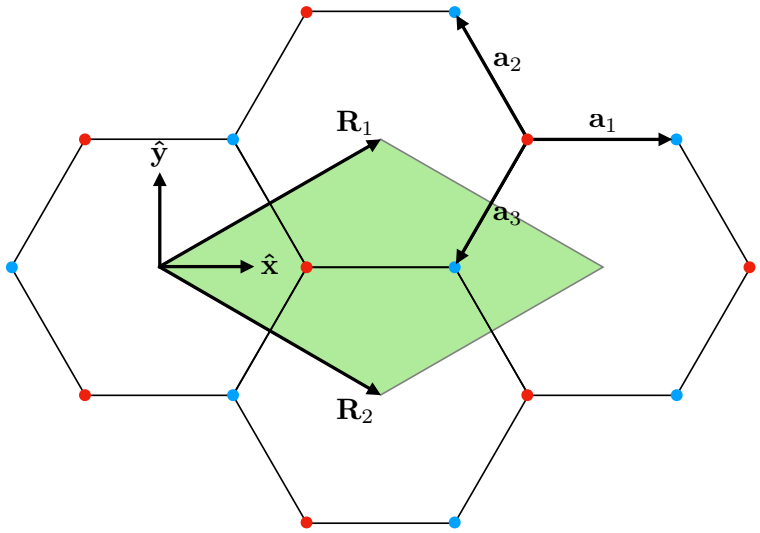

Figure 2.8: Honeycomb lattice for the graphene. It is made of two triangular lattices, sub lattice A (red) and sublattice B (blue).

The primitive vectors $\mathbf{a}_1$, $\mathbf{a}_2$ and $\mathbf{a}_3$, which define the carbon atom's position on the lattice can be defined as

$$\mathbf{a}_1 = a \begin{bmatrix} 1 \\ 0 \end{bmatrix}, \quad \mathbf{a}_2 = \frac{a}{2} \begin{bmatrix} -1 \\ \sqrt{3} \end{bmatrix}, \quad \mathbf{a}_3 = -\frac{a}{2} \begin{bmatrix} 1 \\ \sqrt{3} \end{bmatrix}. \tag{2.53}$$

As we can see from Figure 2.8, graphene can be described as two triangular sublattices, being one defined by the lattice vectors and the other by the primitive vectors.

The Bloch Hamiltonian for graphene is

$$H_0(\mathbf{k}) = \begin{bmatrix} 0 & h(\mathbf{k}) \\ h^*(\mathbf{k}) & 0 \end{bmatrix}, \tag{2.54}$$

where $\mathbf{k}$ is the two dimensional wave vector and

$$h(\mathbf{k}) = t \sum_j e^{i\mathbf{k}\cdot\mathbf{a}_j}, \tag{2.55}$$

where t is the hopping parameter.

It is easy to see, from the definition in Equation 2.54, that the graphene's spectrum is given by $\epsilon(\mathbf{k}) = \pm|h(\mathbf{k})|$.

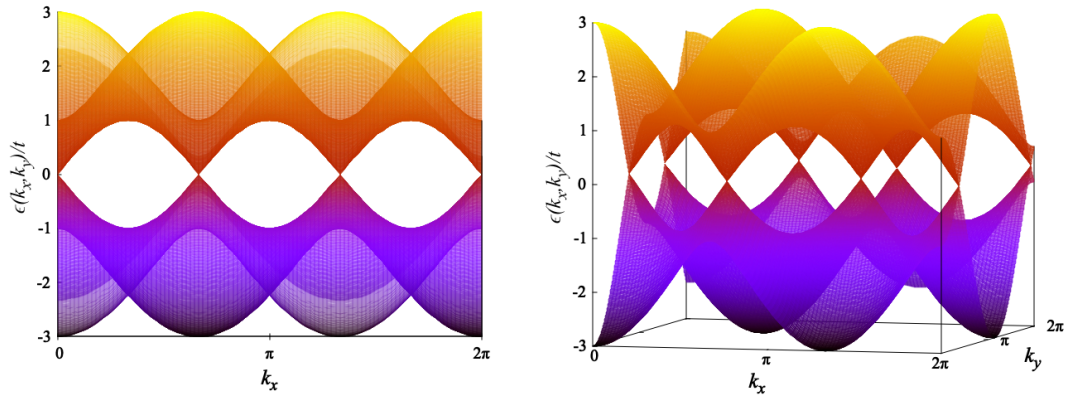

(a) (b)

Figure 2.9: Graphene's bandstructure. In the picture are shown six crossing points that can be separated into two groups of three equivalent points each.

This spinless non-interacting graphene model has no energy gap on its spectrum. The Fermi energy is at $E = 0$, where the spectrum exhibits degenerations. These degeneracies are related to the existence of inversion and time-reversal symmetries. Therefore, if we break one or both of these symmetries, we expect to see an energy gap and a non-trivial Berry curvature. It is necessary to keep in mind that as we are interested in topological insulators, we have to have an insulating system, thus, an energy gap.

It is possible to break inversion symmetry adding two different masses terms for each one of the sublattices. The most common way to do this is as in Equation 2.56,

$$H(\mathbf{k}) = \begin{bmatrix} M & h(\mathbf{k}) \\ h(\mathbf{k})^\dagger & -M \end{bmatrix}. \tag{2.56}$$

The spectrum for this new modified graphene's model is

$$\epsilon(\mathbf{k}) = \pm\sqrt{|h(\mathbf{k})|^2 + M^2}, \tag{2.57}$$

and we can see, in Figure 2.10, that there are no degeneracies.

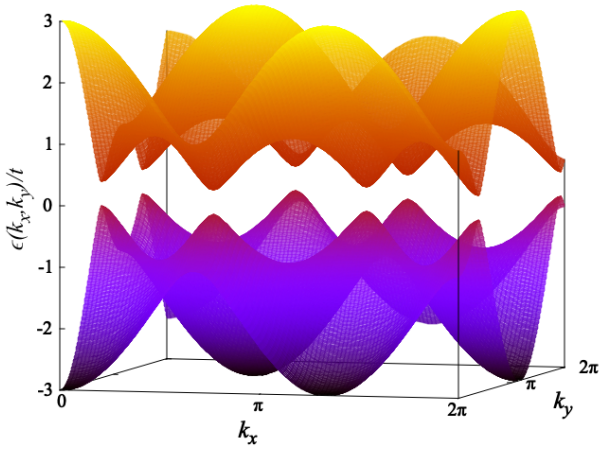

Figure 2.10: Graphene's bandstructure for the case with no inversion symmetry due the presence of a mass term.

If we focus on the eigenstates of this modified graphene model, we will note that for some relation between M and t, there will be localized states on one of the two sublattices. However, there will not be chiral states. The calculation for the Berry phase, and the first Chern number, in this case, gives a value of zero. Therefore, even though there is a gap, the topology for this system is a trivial one. As the addition of a mass term in the Hamiltonian does not provide new topological interesting features, it is convenient to revisit what happens if we break time-reversal symmetry.

Let us take Haldane's idea [6], which consists in adding a second nearest-neighbor hopping, t', and a periodic local magnetic flux density $\mathbf{B}(\mathbf{r})$, normal to the material, with the same symmetries as the lattice and a zero total flux through the unit cell. This new flux adds a phase factor, $\exp(i\phi)$, for the new hoppings, with $\phi = 2\pi(2\Phi_a + \Phi_b)/\Phi_0$, where Φ_a and Φ_b are the regions of the hexagonal cell shown in Figure 2.11 and Φ_0 is the total flux enclosed by a closed path in units of $|h/e|$.

The new hoppings in the system add six new terms in the Hamiltonian. If we label

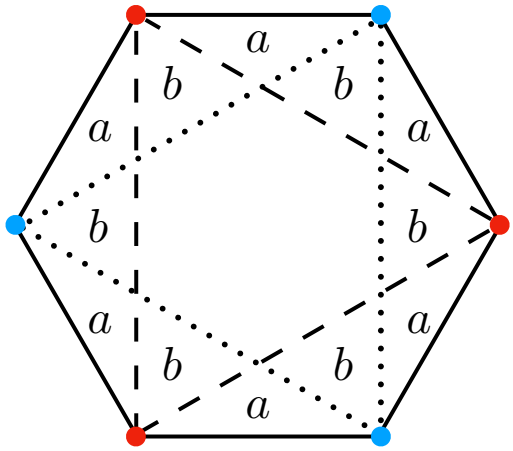

Figure 2.11: Schematic representation for Haldane's graphene model. The solid lines represent the usual nearest-neighbor hoppings and, the dashed and dotted lines represent the second-neighbor hoppings. These hopping will have a different sign phase, as the integrals are performed in opposite directions, for each one of the sublattices.

the vectors pointing to the second nearest-neighbors as $\mathbf{a}_i$, with i going from 4 to 9, the modified Hamiltonian with the mass terms and the new hoppings is

$$H(\mathbf{k}) = \begin{bmatrix} M + j(\mathbf{k}) & h(\mathbf{k}) \\ h(\mathbf{k})^\dagger & -M + j(-\mathbf{k}) \end{bmatrix}, \tag{2.58}$$

where $j(\mathbf{k})$ is given by

$$j(\mathbf{k}) = 2t' \sum_{i=4}^{9} \cos(\phi + \mathbf{k} \cdot \mathbf{a}_i). \tag{2.59}$$

Now we can calculate the first Chern number, for this new modified graphene model, with second nearest-neighbor hoppings. In this case, there will be three different possible results, $\nu = 1$, $\nu = -1$ and, $\nu = 0$. The result obtained will depend on the value of t'. If we look at the spectrum and change the value of it, adiabatically, we will see the gap size will change and, it will close at $t' = \pm M/3\sqrt{3}$. If we continue to evolve the value of t', in the same direction we are doing it, we will re-open the gap. Depending, also, on the value of ϕ, the fact to close and re-open the gap will lead to a phase transition, in this case, a topological one. The topologically interesting cases are those with $\nu \neq 0$, where the system will be in a QHE phase. The phase diagram for this model, depending on the values of t'

and ϕ, is shown in Figure 2.12.

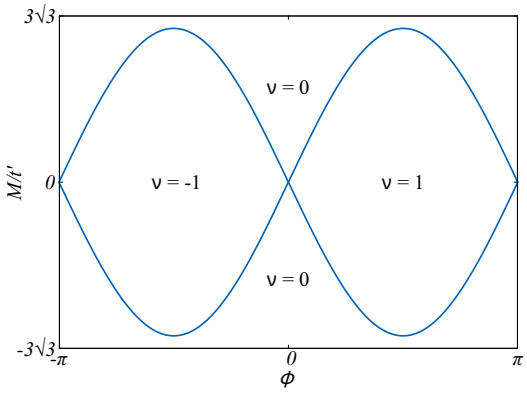

Figure 2.12: Phase diagram for the first Chern number in the Haldane model, depending on the values of ϕ and M/t'.

The Berry phase, and therefore the first Chern number, is defined only for *well defined bands*, which is not the case for a gapless system. As the Berry phase is obtained using the eigenstates of the system, at the degeneracy point, it is possible to "jump" from one eigenstate into another. For a non-trivial topology, graphene should exhibit edge states, which could be different depending on the border, as it could be zig-zag or armchair.

As we have discussed in the previous sections, the topological quantity that we calculate provides information about some physical properties of the system, as the conductance's quantization or the existence of chiral states. The calculation for the Berry phase, or the first Chern number, is only possible for a system with well-defined bands, where a change in the invariant will be a sign of a topological phase transition. It is necessary to remark that a different topological invariant from two systems will indicate that those systems are not topologically equivalent. For the Haldane model, we note that different topologies emerge depending on the relation of its parameters. However, we are missing an important issue. Our work is about topological phase transitions in one dimension and if we look at the Berry phase's definition, we will note that it is not possible to calculate it as it is not possible to perform a simple closed path in one dimension. To solve this "problem", before getting into the details of our work, we are going to analyze the SSH model, the most known and studied one-dimensional topological insulator [7, 8].

2.6 The SSH Model: A One-Dimensional Topological Insulator

The SSH model describes a one-dimensional spinless topological insulator. It is a simple tight-binding model with two staggered hopping amplitudes, as shown in Figure 2.13. An unusual feature of the model, when compared with the previous two-dimensional ones, is the fact that the topological phase transition, or its topology, will not depend on the time-reversal symmetry breaking, but only on the inversion symmetry breaking. Another well-known system whose topology does not need the break of time-reversal symmetry is the Kane and Mele model [9–11], which is the Haldane model, doubled as they add spin. Models as these are known as time-reversal invariant topological insulators. In one dimension, there will no be chiral states as in the Haldane model but edge/end states, which are states localized at the ends of the chain.

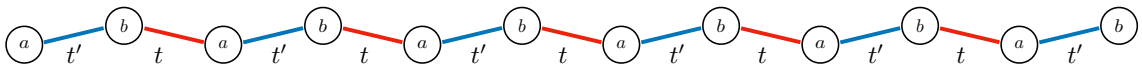

Figure 2.13: Graphic representation for the SSH model. Each unit cell is composed of two sites, a, and b. Thus, it can be represented as a composition of two sublattices A and B. The hopping parameters are staggered, with $t \neq t'$.

The lattice Hamiltonian for the SSH model, in the real space, is given by

$$\hat{H} = -\sum_{n=0}^{N} \left[t'(a_n^\dagger b_n + b_n^\dagger a_n) + t(a_{n+1}^\dagger b_n + b_n^\dagger a_{n+1}) \right]. \tag{2.60}$$

Here the operator $a_n^\dagger$ ($b_n^\dagger$) creates a particle at the n-th site of the sublattice A (B) and the operator a_n (b_n) annihilates a particle at the n-th site of the sublattice A (B). As we already mentioned, t and t' are the hopping parameters which are different[3].

[3]For the case $t = t'$ there's no energy gap. The system is a trivial conducting chain.

Thus, the bulk Hamiltonian in the reciprocal space is

$$H(k) = -\begin{pmatrix} 0 & t' + te^{ika} \\ t' + te^{-ika} & 0 \end{pmatrix}, \tag{2.61}$$

and is related to the lattice Hamiltonian by

$$\hat{H} = \sum_k \Psi_k^\dagger H(k) \Psi_k, \tag{2.62}$$

where

$$\Psi_k^\dagger = \frac{1}{N} \sum_{n=1}^{N} e^{-ikna} \left(a_n^\dagger, b_n^\dagger \right), \tag{2.63}$$

with N being the number cells, in the real space, and a is the lattice constant.

The energy spectrum for the bulk Hamiltonian is

$$\epsilon_\pm(k) = \pm\sqrt{t^2 + t'^2 + 2tt'\cos(ka)}, \tag{2.64}$$

therefore, it is a two band spectrum with the gap $\Delta = 2|t - t'|$, as we can see in Figure 2.14.

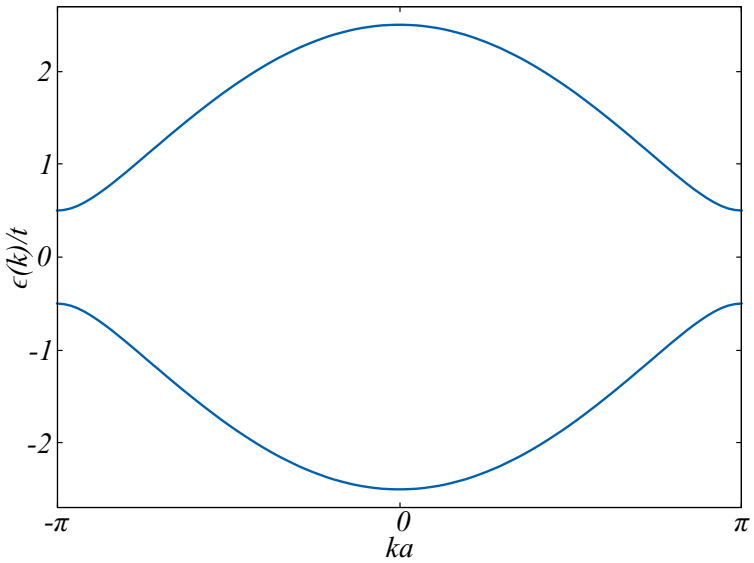

Figure 2.14: Band Structure for the SSH model. Here we have choose $a = 1$ and $t' = 1.5t$. The energy values have been normalized according to the value of t.

And the eigenvectors of $H(k)$ are

$$u_{\pm}(k) = \frac{1}{\sqrt{2}} \begin{pmatrix} \pm \dfrac{e^{ika}\sqrt{t^2 + t'^2 + 2tt'\cos(ka)}}{e^{ika}t' + t} \\ 1 \end{pmatrix}. \tag{2.65}$$

With the eigenvectors, as we already discussed, it is possible to obtain the Berry connection, and, subsequently, the Berry phase. For the first one, there are no complications, but as we already mentioned at the end of the previous section, it is not possible to calculate the Berry phase in one dimension. The solution for this issue was proposed for the first time by Joshua Zak and is known, nowadays, as the Zak phase [12].

2.6.1 The Zak Phase

Let us recall the definition of the Berry phase. It is obtained as the integral of the Berry connection over a simple closed loop. The Berry connection is defined as the inner product between $\langle u_{n\mathbf{k}}|$ and $|\nabla_{\mathbf{k}} u_{n\mathbf{k}}\rangle$. As we are working in one dimension, the gradient becomes a partial derivative and the wavevector $\mathbf{k}$, is replaced by the wavenumber k. Therefore, we have

$$\langle u_{n\mathbf{k}}|\nabla_{\mathbf{k}} u_{n\mathbf{k}}\rangle \quad \rightarrow \quad \langle u_{nk}|\partial_k u_{nk}\rangle\,. \tag{2.66}$$

The solution presented by Zak, to be able to calculate a Berry phase for a one-dimensional system, used the Brillouin zone's periodicity. If the Berry phase is calculated on the Brillouin zone, the initial and the final point can be considered as the same point, due to the periodicity of the space. Therefore, the Berry phase in one dimension, or the Zak phase, is

$$\gamma_n = i \int_{\mathbf{BZ}} \langle u_{nk}|\partial_k u_{nk}\rangle\, dk. \tag{2.67}$$

Just as the Berry phase gives useful information about the topology of the system, the Zak phase will be helpful to learn about the topology of a one-dimensional crystal. If we modify the parameters of a system like the SSH model, in such a way that the energy gap closes and it is re-opened, a $\pm n\pi$ Zak phase's shift, with n being an odd number, will

indicate a change in the topology, a topological phase transition. For one of these two possible topologies, we will have end modes, which are protected as long as the topology remains unchanged. Even though the Zak phase gives us relevant information about the topology of a system, there are some issues we need to clarify before a more in-depth analysis.

Zak Phase Quantization

Just like we studied for the QHE and the conductance's quantization for the Haldane model, it is possible to study the Zak phase's quantization. This quantization is possible if the system has inversion symmetry [4]. It is possible to use the Wannier functions to define the Bloch functions as [12, 13]

$$u_{nk}(x) = \sum_m e^{-ik(x-ma)} W_n(x - ma). \tag{2.68}$$

Therefore, it is possible to see that there is a relation between the Zak phase and the spatial symmetry of the system. More specifically, the Zak phase can be obtained from the calculation of the Wannier center of the crystal as

$$\gamma_n = \frac{2\pi}{a} \int_{-\infty}^{\infty} x |W_n(x)|^2 dx. \tag{2.69}$$

The Zak phase will only take the values 0 or π, modulo 2π, depending on the existence of spatial inversion symmetry. The π difference from a phase and another will indicate different topologies. However, there are two significant issues that it is necessary to review, the Gauge dependence, of the Zak phase and, how to assure the existence of edge states from the Zak phase's value.

Gauge Dependence of the Zak Phase

As we already discussed, the Berry phase is gauge independent. Therefore, it is easy to distinguish a trivial topology from a non-trivial topology. A non-zero Berry phase is

[4] A spinfull system will require **Mirror** symmetry

associated with non-trivial topologies. However, due to the Zak phase's gauge dependence, this is not the case [14]. Let us take $|\tilde{u}_{nk}\rangle$ defined as

$$|\tilde{u}_{nk}\rangle = e^{-ikb} |u_{nk}\rangle , \tag{2.70}$$

the Berry connection is

$$\begin{aligned} \tilde{\mathcal{A}}(k) &= i \langle u_{nk}|\partial_k u_{nk}\rangle + b, \\ \tilde{\mathcal{A}}(k) &= \mathcal{A}(k) + b, \end{aligned} \tag{2.71}$$

and, therefore, the Zak phase is

$$\tilde{\gamma}_n = \gamma_n + \frac{2\pi b}{a}. \tag{2.72}$$

Zak phase's gauge dependence is an essential issue as, even though it is quantized, the value obtained for it is not going to be sufficient to determine if the system's topology is trivial or non-trivial. The only thing that we can learn from it is if there is a topological phase transition if, near the critical point where the gap closes, there is a phase shift of $\Delta\gamma_n = m\pi$, with m an odd number. As we are going to see in the next chapter, the same topology can have different values for the Zak phase. Therefore, for a correct analysis of the topological phases transitions, we will need to see what happens near the critical point. On the other hand, the last issue we have to note is the fact that as we can not distinguish two different topologies just with the Zak phase's value, we will not be able to assure if there are or not, edge states. To understand this in a more explicit form, we are going to discuss the Zak phase and the existence of edge states in the SSH model.

2.6.2 Zak Phase for the SSH model

As we already saw earlier, for $t \neq t'$, there is an energy gap. Thus we can calculate the Zak phase for two cases, $t < t'$ and $t > t'$. Let us take the SSH's eigenstates in Equation 2.65, normalized to avoid possible errors. The result, for the Zak phase in both

cases, is

$$\gamma = \begin{cases} 0, & \text{for} \quad t' < t \\ \pi, & \text{for} \quad t' > t \end{cases}, \tag{2.73}$$

where the result does not depend on the band selection, as both eigenstates return the same value.

The obtained values, for the Zak phase, are constant as long as the ratio t/t' remains smaller or higher to 1. Therefore, if we calculate the Zak phase as a function of t', we will get a value of 0 for $t' < t$ and a value of π for $t' > t$. The phase shift, or jump, will be at $t' = t$, where the Zak phase gives no information about the topology. That is the critical point, where the topological phase transition takes place. We know from these results that there is a topological phase transition, but as we already discussed, we can not know which topology is trivial and which is non-trivial. Therefore, it is necessary to study the finite system to look for edge states.

2.6.3 The Edge States

As we already discussed, the non-trivial topologies for the QHE exhibit chiral states at the sample's edges. If we want to study the edge states, it is necessary to define a finite chain. However, as the SSH model has two sites per unit cell, there is more than one possible open border chain. Therefore, it is necessary to study these possible definitions. As we know, the bulk Hamiltonian is periodic. However, when mapped into the real space, we move into an open border system, as illustrated schematically in Figure 2.15. If we open the chain, as in 2.15(a), the finite chain obtained will have inversion symmetry (as in the Haldane model) and, we can get two values for the Zak phase depending on the relation of t and t', there will be edge states at the ends of the chain for one of the cases. The topological phase transition will create or destroy the edge states. On the other hand, if we look at the Hamiltonian in Equation 2.60, we will note that there is a $(n+1)$ site. Therefore, in that case, we get a chain with an odd number of sites with different hoppings connecting the end sites, thus a non-symmetric chain. In this case, we will have edge states at one end or the other, depending on the relation between t and t'. As this chain is obtained directly from the bulk Hamiltonian, we get the same result as above for the Zak

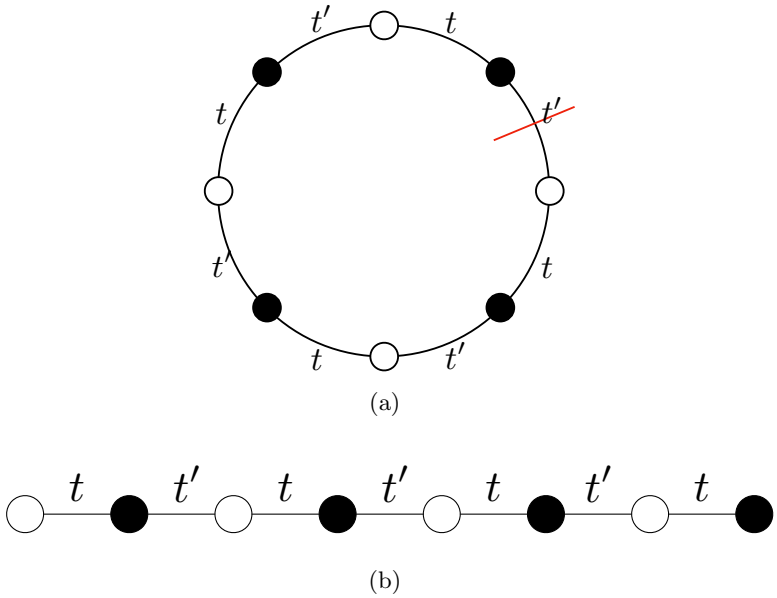

Figure 2.15: Border conditions for the SSH model. The figure in (a) corresponds to an SSH chain with periodic border conditions. If we open the link at the red line, we get an open border chain, like the one in (b). The open border chain has inversion symmetry at the central link.

phase. However, the result of the Zak phase means nothing in this case. The answer to why we obtain two "different topologies" when calculating the Zak phase for this system but no different boundary effects, as we expected, is because the finite chain has no inversion symmetry and, hence, the Zak phase is not quantized. Thus, this non-symmetrical chain is not the right choice for Equation 2.61. We have to keep in mind that as we are studying the bulk-edge correspondence, it is not possible to think about the bulk and the border conditions for the open system separately. It is essential to fix the boundary conditions before the calculation of the Zak phase.

Finally, one last unreviewed issue is about the spectrum and the edge states in the finite system, with inversion symmetry. If we plot the energy for both topologies, as in Figure 2.16, we will note that for the non-trivial, there will be two energy zero states, which are the edge states. As we already discussed before, as long as we do not change the topology, the edge states will remain there. The edge states are topologically protected. As for these states, it is possible to see in Figure 2.17 how is their probability density and how they rapidly decay as we get into the chain.

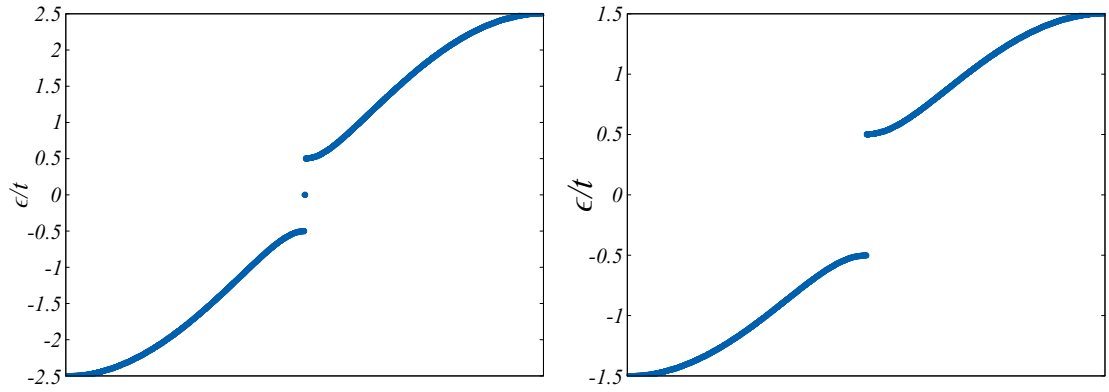

(a) (b)

Figure 2.16: Spectra for the finite SSH chain with inversion symmetry for $N = 500$. In (a) $t' = 1.5t$ and there are two zero energy modes (bound states/end modes). In (b) $t' = 0.5t$ and there are no bound states.

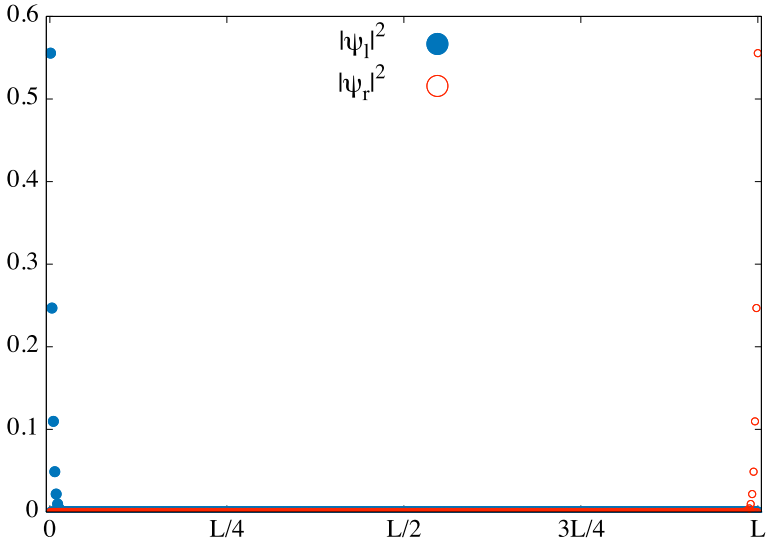

Figure 2.17: Bound States for the SSH model with $N = 500$.

In this chapter, we have discussed the basic notions of topology to be able to recognize a topological phase transition. We have discussed in-depth what is the Berry phase and how to calculate it for 1D systems, where it is known as the Zak phase. Even though some of the aspects discussed here seemed to be unnecessary, we have discussed it as they are going to be notably relevant to understand the basis of this topic, as follows for the gauge dependence of the Zak phase. With all the previous discussion, we are ready to get into

the details of our work about 1D photonic topological insulators.

Chapter 3

1D Topological Insulator for Light

In the previous chapter, we discussed the aspects that turn a regular insulator into a topological one. This chapter, focused on our work, is dedicated to expanding that discussion within the context of photonic crystals. Therefore, we will first introduce the formalism used in this work to describe photonic crystals. Then, we will present the specific model we worked with, and subsequently, we will analyze the topological aspects of the model.

3.1 Photonic Crystals

The electronic band theory, presented in the previous chapter, begins with the Schrödinger equation, a wave equation, within a periodic potential. For physical systems with the same structure, it is possible to build a similar theory. That is the case for the photonic crystals [15–18], which are periodic arrangements of materials with different dielectric constants, which give to the electromagnetic waves a behavior similar to the electrons within a periodic potential.

In Figure 3.1 and Figure 3.2 are depicted two Photonic Chrystals in one and two dimensions. Different colors represent materials with different dielectric constants. The one-dimensional Photonic Crystal in Figure 3.1 is analog to the SSH model, discussed in the previous chapter, and the two-dimensional in Figure 3.2 is analog to a square lattice.

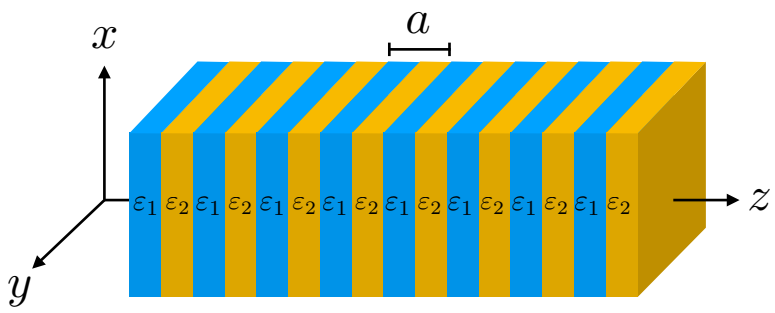

Figure 3.1: Schematic representation of a one-dimensional photonic crystal. Slabs of different dielectric constant are placed alternately in a direction.

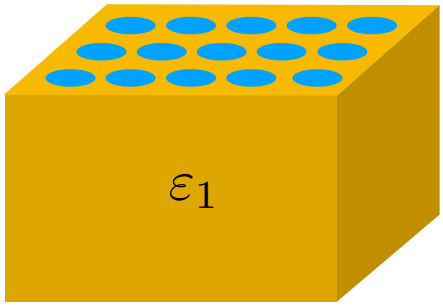

Figure 3.2: Schematic representation of a two-dimensional photonic crystal.

3.1.1 The Maxwell's Equations and the Electromagnetic Wave Equations

It is well known that the physics of classical macroscopic electrodynamics is described by Maxwell's equations, which are [19]

$$\nabla \cdot \mathbf{D}(\mathbf{r},t) = \rho, \tag{3.1}$$

$$\nabla \times \mathbf{H}(\mathbf{r},t) - \partial_t \mathbf{D}(\mathbf{r},t) = \mathbf{J}(\mathbf{r},t), \tag{3.2}$$

$$\nabla \times \mathbf{E}(\mathbf{r},t) + \partial_t \mathbf{B}(\mathbf{r},t) = 0, \tag{3.3}$$

$$\nabla \cdot \mathbf{B}(\mathbf{r},t) = 0, \tag{3.4}$$

where $\mathbf{E}$ is the macroscopic electric field, $\mathbf{H}$ is the macroscopic magnetic field, $\mathbf{D}$ is the electric displacement, $\mathbf{J}$ is the electric current and $\mathbf{B}$ is the magnetic induction, with the constitutive relations $\mathbf{D} = \epsilon(\mathbf{r})\mathbf{E}$ and $\mathbf{B} = \mu(\mathbf{r})\mathbf{H}$. Here, $\epsilon(\mathbf{r}) = \epsilon_0\epsilon_r$ is the electric permittivity ($\epsilon_0 \approx 8.854 \cdot 10^{-12} F/m$ being the vacuum permittivity) and $\mu(\mathbf{r}) = \mu_0\mu_r$ is

the magnetic permeability ($\mu_0 = 4\pi \cdot 10^{-7} H/m$ being the vacuum permeability). It is relevant to address that we have not made any assumptions for none of these parameters.

Without the presence of free charges and no electrical current, which is the case for photonic crystals, Maxwell's equations are simplified,

$$\nabla \cdot \epsilon(\mathbf{r})\mathbf{E}(\mathbf{r},t) = 0, \tag{3.5}$$

$$\nabla \times \mathbf{H}(\mathbf{r},t) - \partial_t \epsilon(\mathbf{r})\mathbf{E}(\mathbf{r},t) = 0, \tag{3.6}$$

$$\nabla \times \mathbf{E}(\mathbf{r},t) + \partial_t \mu(\mathbf{r})\mathbf{H}(\mathbf{r},t) = 0, \tag{3.7}$$

$$\nabla \cdot \mu(\mathbf{r})\mathbf{H}(\mathbf{r},t) = 0. \tag{3.8}$$

Here we have written Maxwell's equations in terms of $\mathbf{E}$ and $\mathbf{H}$ because the photonic crystal's description depends on $\epsilon(\mathbf{r})$ and $\mu(\mathbf{r})$. Thus, we want both parameters explicitly in the equations.

The calculation of the curl of $\mathbf{E}$ and $\mathbf{H}$, using Equation 3.7 and Equation 3.6 results in

$$\nabla \times \left(\frac{1}{\mu(\mathbf{r})} \left(\nabla \times \mathbf{E}(\mathbf{r},t) \right) \right) = -\epsilon(\mathbf{r}) {\partial_t}^2 \mathbf{E}(\mathbf{r},t), \tag{3.9}$$

$$\nabla \times \left(\frac{1}{\epsilon(\mathbf{r})} \left(\nabla \times \mathbf{H}(\mathbf{r},t) \right) \right) = -\mu(\mathbf{r}) {\partial_t}^2 \mathbf{H}(\mathbf{r},t), \tag{3.10}$$

which is an unusual form to write the electromagnetic wave equations as, usually, $\nabla(1/\epsilon(\mathbf{r})) = \nabla(1/\mu(\mathbf{r})) = 0$. If we consider this, we get the usual form of the equations, $({\partial_t}^2 - c^2\nabla^2)\mathbf{A}(\mathbf{r},t) = 0$, where $\mathbf{A}(\mathbf{r},t)$ is the electric/magnetic field.

As we already mentioned, we have not made any restriction on $\epsilon(\mathbf{r})$ and $\mu(\mathbf{r})$, because these parameters will define the topological behavior of our system, as t and t' for the SSH model. Usually, within the subject of photonic crystals, the materials studied are transparent and present no dispersion[1], so ϵ_r is real and positive and, $\mu_r \sim 1$.

It is useful to separate the spatial part of both fields from the time-dependent by

[1]For dispersive materials, the permittivity also depends on the electromagnetic wave's frequency (ω).

expanding the fields into a set of harmonic modes [15]. This leads to

$$\nabla \times \mathbf{E}(\mathbf{r}) = i\omega\mu(\mathbf{r})\mathbf{H}(\mathbf{r}), \tag{3.11}$$

$$\nabla \times \mathbf{H}(\mathbf{r}) = -i\omega\epsilon(\mathbf{r})\mathbf{E}(\mathbf{r}), \tag{3.12}$$

and, therefore, we get

$$\nabla \times \left(\frac{1}{\mu(\mathbf{r})}\nabla \times \mathbf{E}(\mathbf{r})\right) = \omega^2\epsilon(\mathbf{r})\mathbf{E}(\mathbf{r}), \tag{3.13}$$

$$\nabla \times \left(\frac{1}{\epsilon(\mathbf{r})}\nabla \times \mathbf{H}(\mathbf{r})\right) = \omega^2\mu(\mathbf{r})\mathbf{H}(\mathbf{r}). \tag{3.14}$$

If we consider the restrictions mentioned before about the value of the electric permittivity and the magnetic permeability, 3.14 can be rewritten as

$$\boxed{\nabla \times \left(\frac{\epsilon_0}{\epsilon(\mathbf{r})}\nabla \times \mathbf{H}(\mathbf{r})\right) = \left(\frac{\omega}{c}\right)^2 \mathbf{H}(\mathbf{r})}, \tag{3.15}$$

which is known as the master equation and, with the conditions in Equation 3.5 and Equation 3.8, gives the necessary information to solve the problem. It is preferred to solve the problem for the magnetic field as the calculation for the electric field might be a bit more complicated, due to the dependence of the electric permittivity. Now the problem is an eigenvalue problem, with eigenvalues $(\omega/c)^2$. As the electric permittivity is periodic in space, for the cases we are interested in, we can perform an analogous treatment to the band theory in the crystal structure case explained in the previous chapter. Therefore, we can do a similar analysis with an analogous band structure for the frequencies. The formalism introduced here is the most used to describe photonic crystals. However, we will present another form to describe these systems and will show some differences which will be useful to illustrate why to use it instead.

3.1.2 The First Order Schrödinger Formalism for Electromagnetic Waves

We take the *dynamical equations*, Equation 3.6 and Equation 3.7 and rewrite them as

$$\begin{bmatrix} \nabla \times \mathbf{H}(\mathbf{r},t) \\ -\nabla \times \mathbf{E}(\mathbf{r},t) \end{bmatrix} = \frac{\partial}{\partial t} \begin{bmatrix} \epsilon(\mathbf{r})\mathbf{E}(\mathbf{r},t) \\ \mu(\mathbf{r})\mathbf{H}(\mathbf{r},t) \end{bmatrix}. \tag{3.16}$$

As $\epsilon(\mathbf{r})$ and $\mu(\mathbf{r})$ are time-independent, at least in our work, we can rewrite the right-hand side of the equation as the product of a diagonal matrix and the vector with the time derivative for the electric and magnetic macroscopic fields. And it is possible to do something similar for the left-hand side of the equation, rewriting it as the product of an off-diagonal matrix with the curls and the same vector on the right-hand side. Therefore, Equation 3.16 is rewritten as

$$\begin{bmatrix} 0 & \nabla\times \\ -\nabla\times & 0 \end{bmatrix} \begin{bmatrix} \mathbf{E}(\mathbf{r},t) \\ \mathbf{H}(\mathbf{r},t) \end{bmatrix} = \begin{bmatrix} \epsilon(\mathbf{r}) & 0 \\ 0 & \mu(\mathbf{r}) \end{bmatrix} \frac{\partial}{\partial t} \begin{bmatrix} \mathbf{E}(\mathbf{r},t) \\ \mathbf{H}(\mathbf{r},t) \end{bmatrix}. \tag{3.17}$$

Now we can multiply by the inverse of the matrix with the electric permittivity and magnetic permeability at both sides and multiply by the imaginary unit i so we get

$$\begin{bmatrix} \epsilon(\mathbf{r}) & 0 \\ 0 & \mu(\mathbf{r}) \end{bmatrix}^{-1} \begin{bmatrix} 0 & i\nabla\times \\ -i\nabla\times & 0 \end{bmatrix} \begin{bmatrix} \mathbf{E}(\mathbf{r},t) \\ \mathbf{H}(\mathbf{r},t) \end{bmatrix} = i\frac{\partial}{\partial t} \begin{bmatrix} \mathbf{E}(\mathbf{r},t) \\ \mathbf{H}(\mathbf{r},t) \end{bmatrix}. \tag{3.18}$$

The Equation 3.18 now looks like a Schrödinger equation in which the "Hamiltonian" is given by the product of the two matrices at the left hand side. This is,

$$\underbrace{\underbrace{\begin{bmatrix} \epsilon(\mathbf{r}) & 0 \\ 0 & \mu(\mathbf{r}) \end{bmatrix}^{-1}}_{W} \underbrace{\begin{bmatrix} 0 & i\nabla\times \\ -i\nabla\times & 0 \end{bmatrix}}_{D}}_{M} \underbrace{\begin{bmatrix} \mathbf{E}(\mathbf{r},t) \\ \mathbf{H}(\mathbf{r},t) \end{bmatrix}}_{\Psi(\mathbf{r},t)} = i\frac{\partial}{\partial t} \underbrace{\begin{bmatrix} \mathbf{E}(\mathbf{r},t) \\ \mathbf{H}(\mathbf{r},t) \end{bmatrix}}_{\Psi(\mathbf{r},t)} \tag{3.19}$$

$$\boxed{M\Psi(\mathbf{r},t) = i\frac{\partial}{\partial t}\Psi(\mathbf{r},t).} \tag{3.20}$$

As we can see, our Hamiltonian-like operator has first-order derivatives in space. But

the Schrödinger equation has second-order derivatives on it. Therefore we call it *first-order Schrödinger formalism* (FOSF) in contrast to the previous formalism, which we will call *second-order Schrödinger formalism* (SOSF) [20, 21].

Advantages and Disadvantages of the FOSF

It is possible to see that the FOSF has some disadvantages in comparison to the SOSF. The most obvious is the fact that for the SOSF, the magnetic and electric fields are decoupled and, as we already mentioned, we need to solve only one one of the two equations to get the required information. However, there is another relevant disadvantage which is the "non-Hermiticity" of the Schrödinger-like operator.

Why do we use quotation marks when we are talking about this non-Hermiticity? The answer is quite simple. In usual quantum mechanics we are used to say that an operator is hermitian if it is equal to its transposed complex conjugate ($A^\dagger = A$). However, the condition for an operator to be hermitian is given by

$$\langle f| A |g\rangle = \langle g| A |f\rangle^* , \tag{3.21}$$

where f and g are functions in the Hilbert space [22]. This definition is considers the inner product of the Hilbert space, then it is necessary to check the inner product for the FOSF. As we already saw in Eq. (3.19) our operator is defined as the product of two Hermitian operators $M = WD$, thus redefining the inner product as

$$\langle f|g\rangle_W = \langle f| W^{-1} |g\rangle , \tag{3.22}$$

the operator M will fulfil the condition in Eq. (3.21). This is,

$$\langle f| M |g\rangle_W = \langle f| D |g\rangle , \tag{3.23}$$

where D is Hermitian in the "usual form", so $\langle f| D |g\rangle = \langle g| D |f\rangle^*$[2] for the details.

As the redefinition of the inner product solves the "problem of the non-Hermiticity" we

[2]See Appendix F

see no more concerning disadvantages of the FOSF (besides the fact we already mentioned about the fields being coupled).

As we want to construct a band theory for photonic crystals we would like to work with ω instead ω^2, thus the FOSF seems more convenient. However, we could simply calculate the square root for the eigenvalue obtained by the SOSF and get $|\omega|$. If done that, a new problem arises. As the Maxwell's equations solutions for electromagnetic waves exists for $\omega < 0$ and $\omega > 0$ if we get the absolute value of the frequency we are omitting some solutions. A naive guess would be to get that absolute value and chose the negative and the positive values, $\pm\omega$, but that could most certainly lead to a wrong result. A graphic example is shown in Figure 3.3. It is easy to see from this example the arising problem

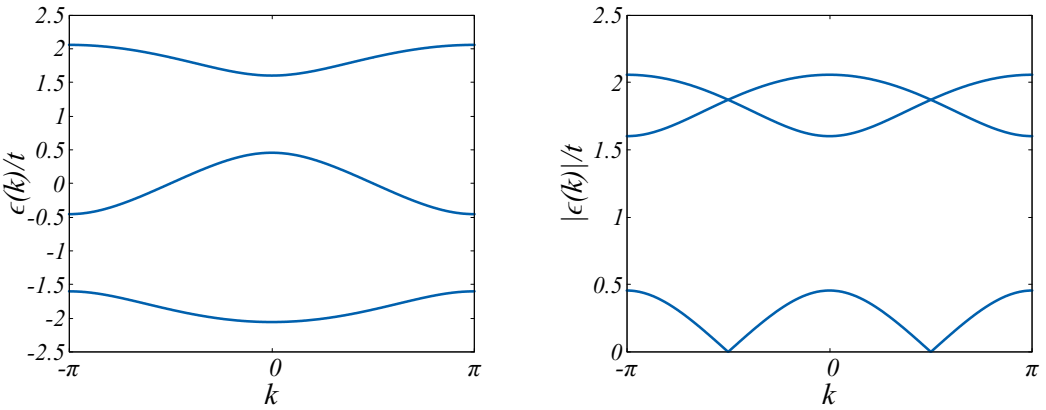

Figure 3.3: Energy Band Structure of a three sites per unitary cell chain. (a) shows $\epsilon(k)$ and (b) shows the absolute value of $\epsilon(k)$

when the alternative to use $\pm\omega$ is chosen.

The necessity to have a well-defined band structure relies in the fact that the topological aspects we want to study are in the band structure of the system. If we do not have a well constructed band structure this would most likely lead us to wrong results and interpretations. Crossing points that does not exists in the actual system or band gaps of wrong range are examples of misleading facts.

Even though we are motivated to construct a well-defined band structure for photonic crystals we have not discussed yet the physical meaning of such structure. The *frequency*

band structure, in the same way as for electrons, shows the frequency of light modes propagating through the photonic crystal. Thus the photonic band gap shows the frequencies of electromagnetic waves which won't be transmitted through the crystal, i.e. those electromagnetic waves will be reflected from the crystal.

3.2 The Model

As we mentioned in chapter 1, we are going to study the topological behaviour of a 1D photonic crystal using the formalism detailed in chapter 2. The 1D photonic system is as the one showed in Figure 3.1. We are interested in the problem of light propagating in $\hat{z}$ direction thus the $\hat{z}$-component of the electric and the magnetic field are both zero. Moreover, as electric and magnetic fields are perpendicular for an electromagnetic wave we can choose a reference frame defined by $\mathbf{E}_1(\mathbf{r},t)$ and $\mathbf{H}_2(\mathbf{r},t)$ which do not change in direction. This is,

$$\begin{bmatrix} E_1(\mathbf{r}) \\ E_2(\mathbf{r}) \\ E_3(\mathbf{r}) \\ H_1(\mathbf{r}) \\ H_2(\mathbf{r}) \\ H_3(\mathbf{r}) \end{bmatrix} \rightarrow \begin{bmatrix} E_1(\mathbf{r}) \\ 0 \\ 0 \\ 0 \\ H_2(\mathbf{r}) \\ 0 \end{bmatrix} \rightarrow \mathbf{\Psi} \equiv \begin{bmatrix} E_1(\mathbf{r}) \\ H_2(\mathbf{r}) \end{bmatrix}. \tag{3.24}$$

As we rewrite our 6-vector as a 2-vector, we can do the same for our 6×6 matrix to get a 2×2 matrix, for simplicity.

$$\begin{bmatrix} 0 & 0 & 0 & 0 & -i\partial_z & i\partial_y \\ 0 & 0 & 0 & i\partial_z & 0 & -i\partial_x \\ 0 & 0 & 0 & -i\partial_y & i\partial_x & 0 \\ 0 & i\partial_z & -i\partial_y & 0 & 0 & 0 \\ -i\partial_z & 0 & i\partial_x & 0 & 0 & 0 \\ i\partial_y & -i\partial_x & 0 & 0 & 0 & 0 \end{bmatrix} \rightarrow D \equiv \begin{bmatrix} 0 & -i\partial_z \\ -i\partial_z & 0 \end{bmatrix}. \tag{3.25}$$

And finally, for the 1D case, matrix W will be given by the 2×2 matrix,

$$W = \begin{bmatrix} \epsilon(z)^{-1} & 0 \\ 0 & \mu(z)^{-1} \end{bmatrix}. \tag{3.26}$$

Thus a 1D Photonic crystal is described by the equation

$$\begin{bmatrix} \epsilon(z)^{-1} & 0 \\ 0 & \mu(z)^{-1} \end{bmatrix} \begin{bmatrix} 0 & -i\partial_z \\ -i\partial_z & 0 \end{bmatrix} \begin{bmatrix} E_1(\mathbf{r}) \\ H_2(\mathbf{r}) \end{bmatrix} = \omega(k) \begin{bmatrix} E_1(\mathbf{r}) \\ H_2(\mathbf{r}) \end{bmatrix}. \tag{3.27}$$

Then, we can build a 1D lattice model using the techniques of the tight binding method, where the hopping elements are given by the inner product of two nearest neighbours and the Hamiltonian. Then, for a 2-periodic system we will have the bulk "Hamiltonian"

$$\mathcal{H}(k) = \begin{pmatrix} 0 & 0 & -i\alpha_1 & i\alpha_1 e^{ika} \\ 0 & 0 & i\beta_1 & -i\beta_1 \\ i\alpha_2 & -i\alpha_2 & 0 & 0 \\ -i\beta_2 e^{-ika} & i\beta_2 & 0 & 0 \end{pmatrix}. \tag{3.28}$$

And according to chapter 2 the redefinition of the inner product is given by $\langle f| A |g\rangle_W = \langle f| W^{-1} A |g\rangle$, with

$$W^{-1} = \begin{pmatrix} \alpha_1^{-1} & 0 & 0 & 0 \\ 0 & \beta_1^{-1} & 0 & 0 \\ 0 & 0 & \alpha_2^{-1} & 0 \\ 0 & 0 & 0 & \beta_2^{-1} \end{pmatrix}. \tag{3.29}$$

3.3 Topological Phase Transitions for the 1D Photonic Topological Insulator

To find the existence of topological phase transitions in our 1D system it is necessary to keep in mind what we already know about these phase transitions and the symmetries of the system, such as chiral symmetry [23, 24]. For the case of the SSH model, in chapter 2, there is no need to impose this symmetry as the system is naturally time-reversal and

chiral symmetric. There is chiral symmetry if the condition $\mathcal{C}\mathcal{H}(k)\mathcal{C}^{\dagger} = -\mathcal{H}(-k)$, where $\mathcal{C}$ is an anti-unitary operator that operates as

$$\mathcal{C}\begin{bmatrix}\phi_n^A\\ \phi_n^B\\ \phi_n^C\\ \phi_n^D\end{bmatrix} = \begin{bmatrix}\phi_n^{*A}\\ -\phi_n^{*B}\\ \phi_n^{*C}\\ -\phi_n^{*D}.\end{bmatrix} \tag{3.30}$$

On the other hand, another natural symmetry of this system is the temporal inversion symmetry, which exists when the relationship $\mathcal{T}\mathcal{H}(k)\mathcal{T}^{\dagger} = -\mathcal{H}(k)$, where $\mathcal{T}$ is also an anti-unit operator that fulfill the condition

$$\mathcal{T}\begin{bmatrix}\phi_n^A\\ \phi_n^B\\ \phi_n^C\\ \phi_n^D\end{bmatrix} = \begin{bmatrix}\phi_n^{*A}\\ \phi_n^{*B}\\ \phi_n^{*C}\\ \phi_n^{*D}.\end{bmatrix} \tag{3.31}$$

Since our system has these two symmetries naturally, it is expected that there are transitions of topological phases. The important question is under what condition these transitions exist.

Since we have 4 free parameters in our Hamiltonian, $\alpha_1, \beta_1, \alpha_2, \beta_2$, the space to search under what conditions these phase transitions exist is a complex task. Since our system has the two symmetries mentioned above, we note that it has similarities with topological insulators as in the case of the SSH model, discussed in the chapter 2. Based on this model, it is possible to assume that the Zak phase is a good candidate of topological invariant to characterize the possible phase transitions of this system so that we proceed to study the cases for which there is spatial inversion symmetry. However, given that the system in question has more degrees of freedom (in terms of the parameters) than the SSH, it is important to note that such symmetry can be even or odd. Even symmetry is obtained under the condition $\alpha_1 = -\beta_2 \neq \beta_1 = -\alpha_2$, while the odd one is obtained with the condition $\alpha_1 = \beta_2 \neq \beta_1 = \alpha_2$ and given the nature of our model (since $\epsilon(z)$ and $\mu(z)$ is

positive) is that we proceed to study the case of odd space inversion symmetry.

3.3.1 Topological Phase Transitions for the Odd Symmetrical 1D Photonic Topological Insulator

Having the conditions for the aforementioned parameters, $\alpha_1 = \beta_2 \neq \beta_1 = \alpha_2$, considerably reduces the freedom of choice of these, so that the system resembles the SSH model. We can say analogously $\alpha_1 = \beta_2 \equiv t$ and $\beta_1 = \alpha_2 \equiv t'$, so that we are only concerned about the reason between these parameters.

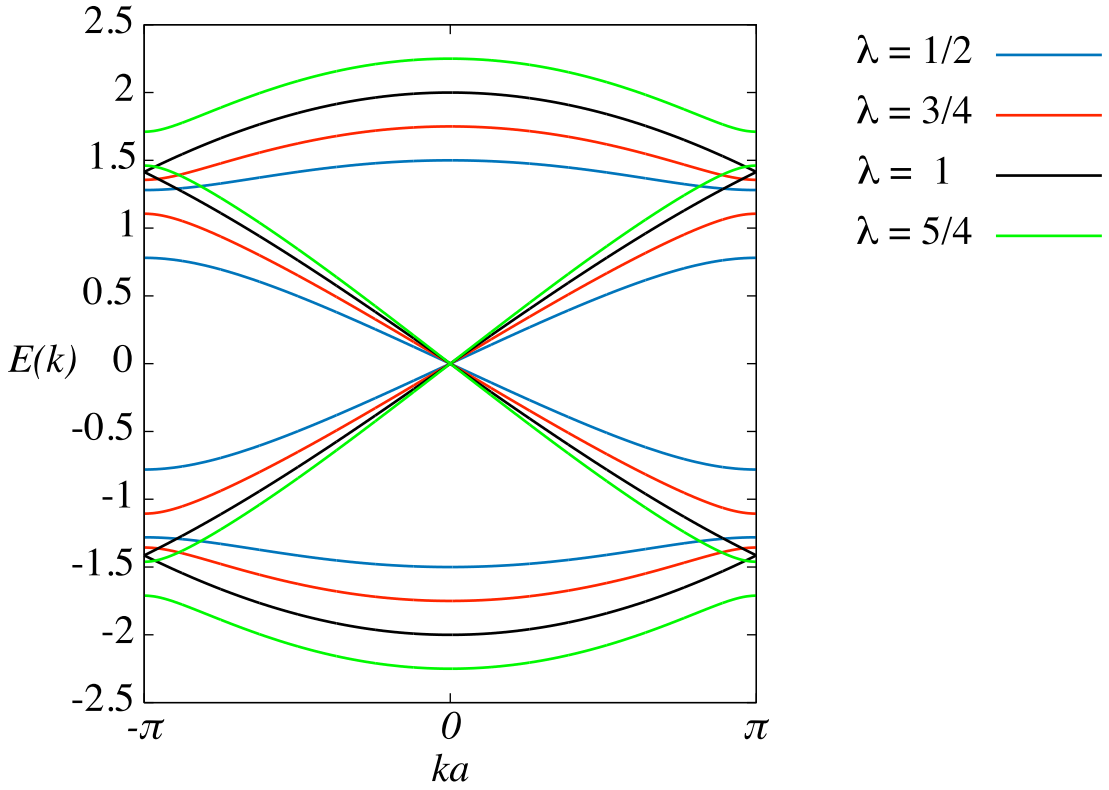

Figure 3.4: Band structure of our model for different values of λ. For $\lambda = 1$ there are no gaps and the Hamiltonian is Hermitian.

In the Figure 3.4 we can see the spectrum of $\mathcal{H}(k)$ for $\alpha_1 \equiv \lambda$ and $\alpha_2 \equiv 1$. We note that for the reason $\alpha_1/\alpha_2 \neq 1$ there are gaps and as we approach $\lambda = 1$ it begins to close, so that when crossing that point we must have passed from a topology to another, that is, at that point there is a topological phase transition.

To verify that it is, indeed, a topological phase transition is that we calculate the Zak phase. However, it is important to note that we must now calculate it using the redefinition of the inner product. This is,

$$\gamma_n = i \int_{\mathbf{BZ}} \langle u_{nk} | \partial_k u_{nk} \rangle_W \, dk. \tag{3.32}$$

It is important to note that we can only calculate the Zak phase for the upper and lower bands, the crossing point between the two remaining bands makes no sense of the value obtained from them, due to the arbitrariness of the way forward when integrating.

In this way, we obtain that for both bands there is a phase transition characterized by a $|\Delta\gamma| = \pi$, as seen in Figure 3.5.

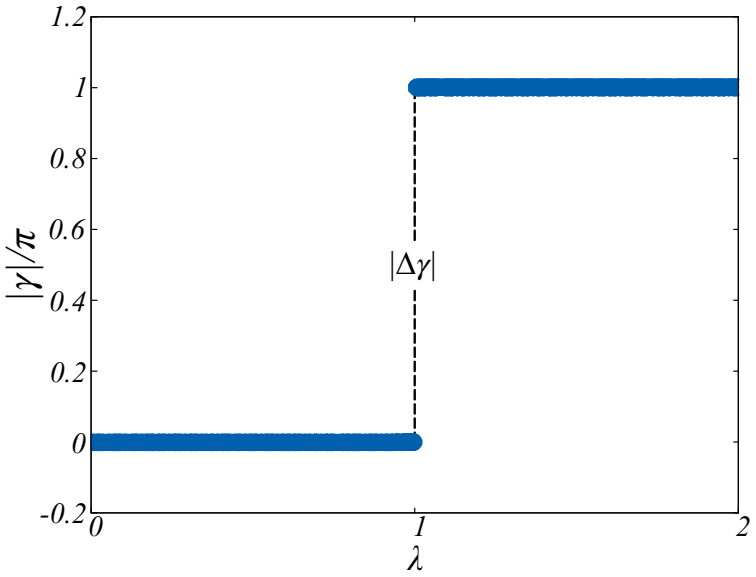

Figure 3.5: Results for the Zak phase's calculation as a function of λ.

Thus, we note that there must indeed be a topological phase transition, as expected, at the point $\lambda = 1$. This implies that there must be topologically protected end states in one or both cases (remember that as mentioned in chapter 2, the existence of the border states also depends on how the borders are).

The chain showed in Figure 3.6 was built with 401 sites so that the number of sites is the same, on both sides, from the center of spatial symmetry. In the case of removing a site, there are only two border states, one with positive frequency and one with negative

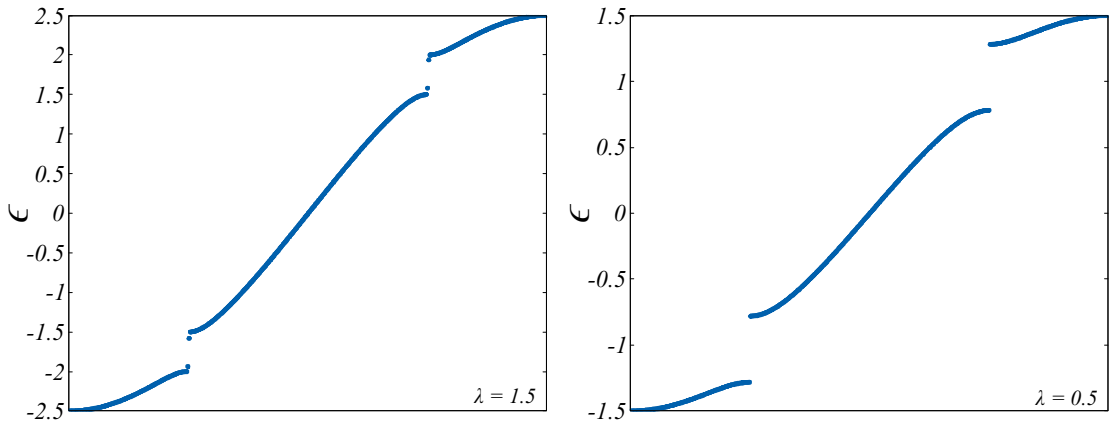

Figure 3.6: Eigenvalues for a 401 sites chain (100 cells). In (a), for $\lambda = 1/2$ it is possible to see that there are 4 gap states. In (b), for $\lambda = 2$, there are no gap states

frequency, as expected as presented in the chapter 2. These states change their edge when they pass through the critical point, as we said was the case with the SSH model in the chapter 2.

To verify that these states are robust, as expected, we can do tests by adding disorder to the system. We do this, for example, by putting small, random site energies.

If we compare the states that live within the crystal for cases with and with no disorder, we note that these can be radically different, as seen in the Figure 3.7.

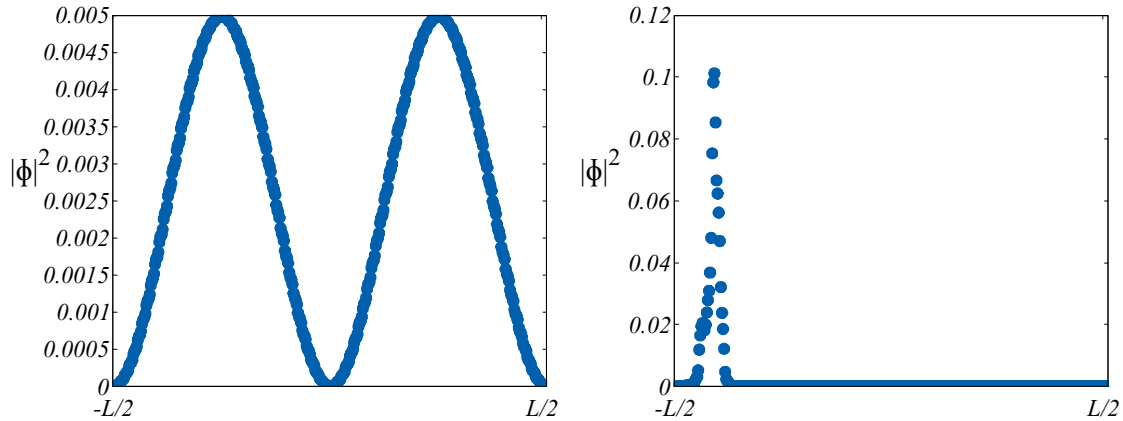

Figure 3.7: Results for $|\phi|^2$ for the cases with disorder (a) and with no disorder (b).

On the other hand, as shown in Figure 3.7, border states do not appear to show significant differences. This coincides with the idea that these states are robust under

disturbances.

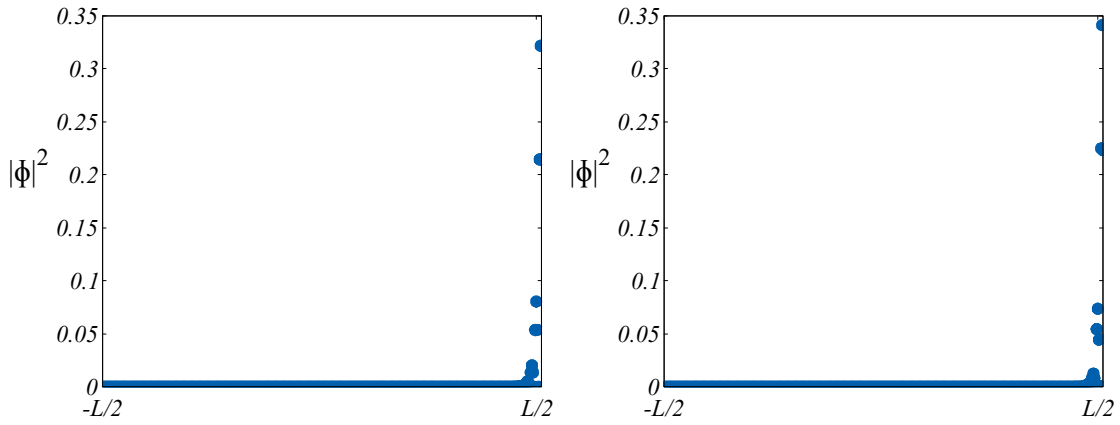

Figure 3.8: Results for $|\phi|^2$ for the cases with disorder (a) and with no disorder (b).

On the other hand, it is necessary to highlight the fact that the symmetry of spatial inversion studied is designed for the bulk. If we look at the finite chain, this is through expansion

$$\hat{H} = \sum_k \Psi_k^\dagger \mathcal{H}(k) \Psi_k, \tag{3.33}$$

where

$$\Psi_k^\dagger = \frac{1}{\sqrt{N}} \sum_{n=1}^{N} e^{ikan} (a_n^\dagger, b_n^\dagger, c_n^\dagger, d_n^\dagger), \tag{3.34}$$

it is possible, in real space, that we could choose other points for which we could choose inversion symmetry.

3.4 The Other Symmetry Points

If we look at the chain in real space, as we mentioned previously, we will see that it has the form shown in the Figure 3.9.

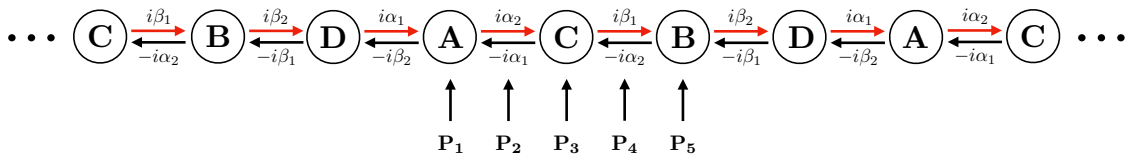

Figure 3.9: Different points around which the chain is symmetrical under inversion symmetry.

Each one of the marked points can be considered a point of symmetry of spatial inversion under different conditions. It is easy to notice that the P_1 point is the same P_5 (due to the periodicity of the system), which is consistent with the fact that if a 1D chain has a point of symmetry, a shift in $a/2$ from that point gives us another point with the same symmetry. The point P_4 turns out to be the point we studied in the previous section, for which only the case of odd symmetry makes physical sense (in principle). In this way, we would have the possibility to study 3 more points in question, for which there are different conditions of symmetry. These conditions are summarized in Figure 3.9.

	$\mathbf{P_1}$			$\mathbf{P_2}$		$\mathbf{P_3}$		
S	$\alpha_1 = 0$	$\beta_1 = 0$	$\alpha_2 = -\beta_2$	$\alpha_1 = -\alpha_2$	$\beta_1 = -\beta_2$	$\alpha_1 = -\beta_1$	$\alpha_2 = 0$	$\beta_2 = 0$
A	α_1 free	β_1 free	$\alpha_2 = \beta_2$	$\alpha_1 = \alpha_2$	$\beta_1 = \beta_2$	$\alpha_1 = \beta_1$	α_2 free	β_2 free

Table 3.1: Conditions for different symmetries depending on the choice of the symmetry point.

As mentioned in the previous section, given the nature of the model in which the jump from one site to other but the reverse have an opposite sign, even symmetry is possible having to define at least one of the parameters as negative, of so that we dismiss these cases in principle. That without considering that for points P_1 and P_3 the fact that some of the parameters are zero, they immediately give us a chain with non-connected sites, so it is trivial.

From the points shown in Table 3.1, we note that there is a certain similarity in the structure of the conditions of the point P_1 and P_3, just as the point P_2 has with P_4. Since the first two have two free parameters, each one, looking for possible transitions of topological phases is again a complex task, so we set it aside for a moment. However, we note that the odd symmetry condition for the point P_2, in real space, delivers the same chain from the previous section, shifted one site.

Although, we have that these two conditions result in the same system in real space and both systems show edge states that appear or disappear when making the variation of the ratio between the Hamiltonian parameters (in the case of the point P_2 the reason is α_1/β_1), when calculating the Zak phase for the condition of point P_2 gives us a completely different result, since the value is not constant for the same topology.

Seeing the variation of the Zak phase based on the evolution of the parameters, in

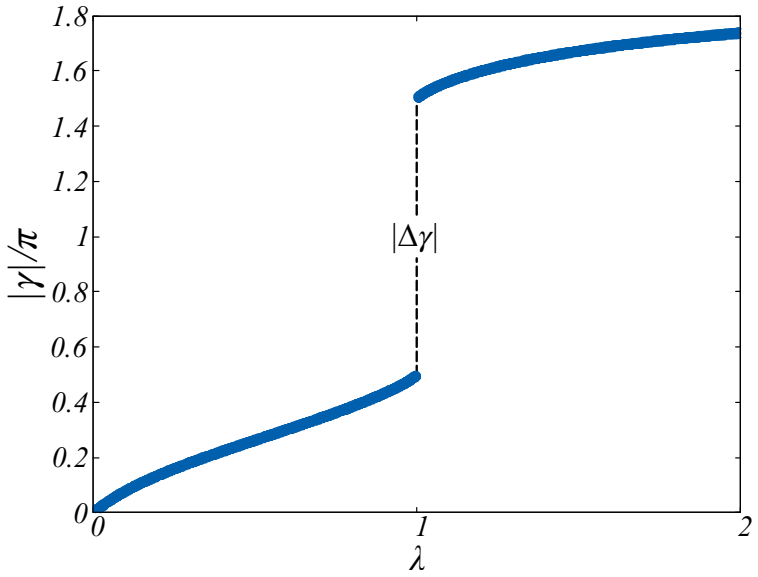

Figure 3.10: Zak phase's value for the odd symmetry condition at point P_2 as a function of the ratio α_1/α_2.

Figure 3.10, we note that the discontinuity produced at $\alpha_1/\alpha_2 = 1$ is just $|\Delta\gamma| = \pi$, which would be a good indicator that there is, indeed, a topological phase transition. However, the fact that $|\Delta\gamma|$ is not constant for the same topology makes us question whether it is as good a topological invariant as it is usually considered.

3.4.1 Revisiting the Zak Phase's Gauge Dependency

As we discussed in chapter 2, the Zak phase is gauge dependent. However, it has been shown that the shift in the Zak phase is constant [14], instead of having an integer value for the Zak phase for each topology, it has semi-integer values, with π jumps between each of these.

In the work of Rhim et al. [25] we can see a much more complete demonstration about the dependence of the Zak phase on the definition of the unit cell.

Taking a Bloch function, for a system with greater periodicity as in our case, of the form

$$\psi_{n,k}(x) = \frac{1}{\sqrt{N}} \sum_{m}^{N} \sum_{j}^{N_b} \alpha_k^{n,j} \phi(x - ma - b_j a) e^{ikma}, \tag{3.35}$$

where N is the number of cells and N_b the number of sites per cell, it is obtained from

the calculation of the Zak phase is given by an inter-cell term and an intra-cell term, the latter being the usual one. This is,

$$\gamma_n^{intra} = i \sum_j^{N_b} N \int_{\mathbf{BZ}} dk \alpha_k^{n,j*} \partial_k \alpha_k^{n,j}, \tag{3.36}$$

$$\gamma_n^{inter} = N \int_{\mathbf{BZ}} dk \int_{\Omega} dx x |\psi_{n,k}(x)|^2 - 2\pi m_{\Omega}, \tag{3.37}$$

where Ω denotes de unitary cell and m_Ω being the index of that given cell.

Another interesting point of that work is that it is given a physical interpretation, beyond the characterization of a topological phase transition, to the calculation of the Zak phase when related to electrical polarization, as demonstrated by King-Smith and Vanderbilt [13, 26]. However, given the different physical nature of our model, relating this phase to physical phenomena in the same spirit is a pending task.

Understanding that the Zak phase is a slightly more complex amount than the one shown above is that it is possible to use this change in the Zak phase without major concerns as a good indicator of the existence of a topological phase transition.

3.5 The Final Two Symmetry Points

As we mentioned previously, the study concerning the points P_1 and P_3 is complex. The fact that there are two unconstrained parameters is what makes it more challenging than the previous cases. However, after studying what happens in those cases, it is possible to make some considerations to make this more manageable.

First, we note that the restriction for the point P_1 is given by $\alpha_2 = \beta_2$ but for the point P_3 is given by $\alpha_1 = \beta_1$, and the other parameters unconstrained. Therefore, taking both restrictions it is possible to get an odd-symmetrical chain, for both points. Similar to other cases previously noted.

As it is possible to see in Figure 3.11, the Zak phase for this case is constant for any value of the relation between α_1 and α_2, and, when changing the parameters, we reach the point $\alpha_1 = \alpha_2 = \beta_1 = \beta_2$. It implies that we are closing and reopening the gap and, in this process, we get localized border states for one of the cases. It is important to remark

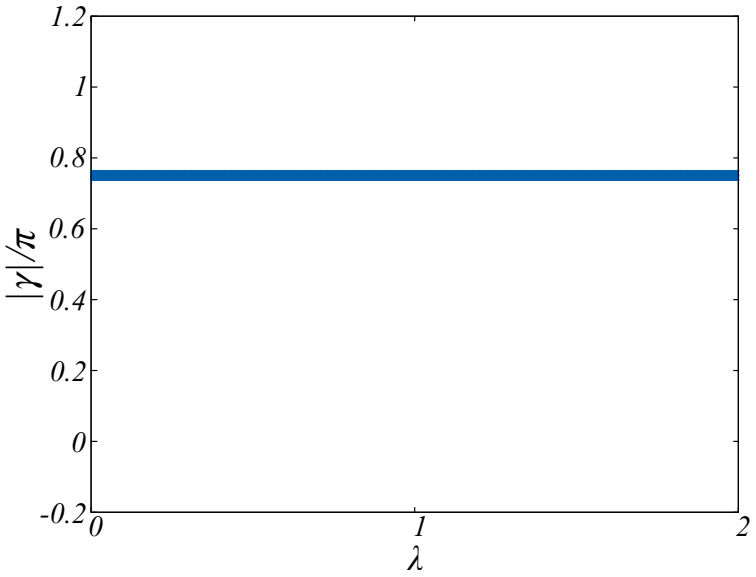

Figure 3.11: Calculation of the Zak phase for the chain with the odd symmetry condition around the point P_1 (or P_3), depending on the ratio between α_1 and β_1.

that the only thing that we could say for this case, noticing that the phase is constant, is that the Zak phase can not tell us anything about a topological phase transition. As we discuss in chapter 2, two topologies are different if at least one invariant is different. The reverse case gives no information about the topologies.

Although this case raises new questions regarding Zak's phase utility as a topological invariant or even concerning the studied system, the solution is much simpler than one might imagine. The chain obtained with these constraints is one of lower periodicity: a trivial one. The emergence of edge states, in this case, would be only due to border effects and would not be related to bulk properties. Those edge states would not be topological.

Finally, there are still two possible cases to review, also for odd symmetry around P_1 and P_3. For the previously discussed conditions, we changed one of the two parameters compared to the other one. Different topologies were obtained around the critical point, given by the ratio of the parameters. Thus, to look for other possible topological phase transitions, we know that we have to look around the critical point, in which the four parameters are equals. Therefore, we can take the condition $\alpha_1 = 1/\beta_1$ for the symmetry around P_1 and $\alpha_2 = 1/\beta_2$ for the symmetry around P_3. Thus when we change the value of those parameters, we cross the critical point.

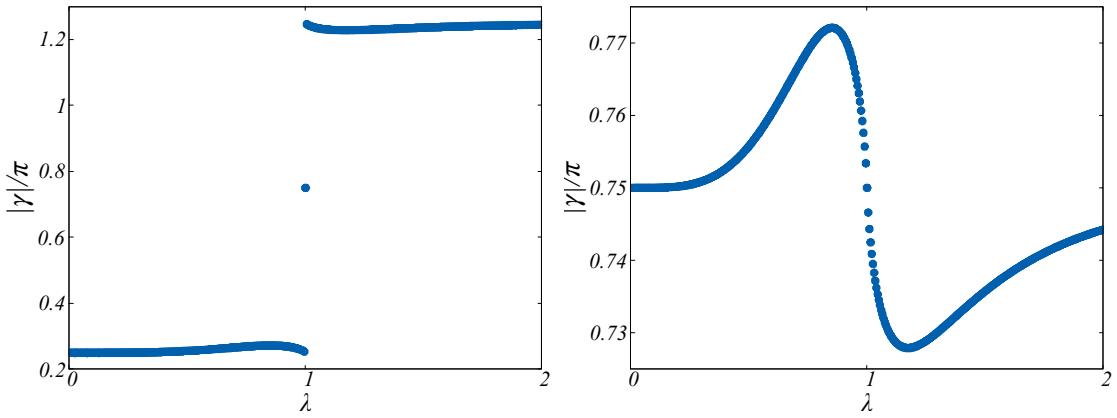

Figure 3.12: Zak phase calculation for chains with odd symmetry around the points P_1 in (a) and P_3 in (b).

Seeing the results obtained for the calculation of the Zak phase, shown in Figure 3.12, we note that for the odd symmetry condition around the point P_1 there is a discontinuity around the critical point and edge states for the case $\alpha_1 < \alpha_2$. A particularity of these edge states is that their frequency takes values at the center of the gap. In other cases, they were located within the limits of these.

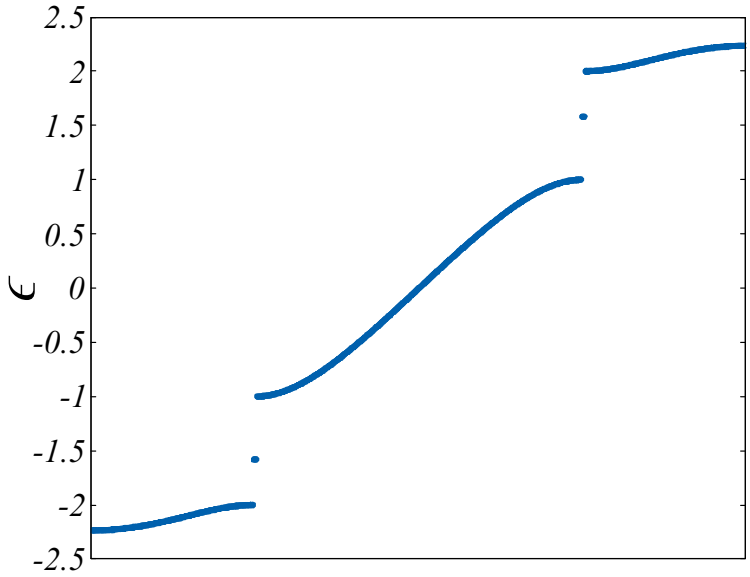

Figure 3.13: Eigenvalues for a 401 sites chain with odd symmetry for the conditions $\alpha_1 = 1/\beta_1 = 1/2$ y $\alpha_2 = \beta_2 = 1$.

For the second case, with $\alpha_2 = 1/\beta_2$, we note that the variation in the Zak phase seems

to have no discontinuities but even though in real space this chain is equal to the other (with the offset of a site as in the first two cases of this chapter), we cannot say with complete certainty that this particular result is produced purely by the gauge dependence of the phase. Due to the above, it is not possible to insure anything regarding this case.

3.6 The Even Symmetries

In previous sections, we dismissed the study for even symmetries because those symmetries are only possible if the electrical permittivity and/or magnetic permeability are negative. That is a problem as the usual materials that we are studying are described with positive parameters. Cases with negative electrical permittivity and/or magnetic permeability are known as *metamaterials*.

It is interesting, as these cases also have localized edge states that appear or disappear as we chain the parameters around a critical point. However, the biggest problem, in this case, is the impossibility of calculating the Zak phase.

The reason for not being able to calculate the Zak phase goes beyond the problem of non-Hermiticity. In the case of the mentioned metamaterials, the spectrum is complex. The topological invariant calculated to study the model is defined for systems with real spectrum. Therefore, it is necessary to find a proper topological invariant to be able to characterize the (possible) different topologies for these cases.

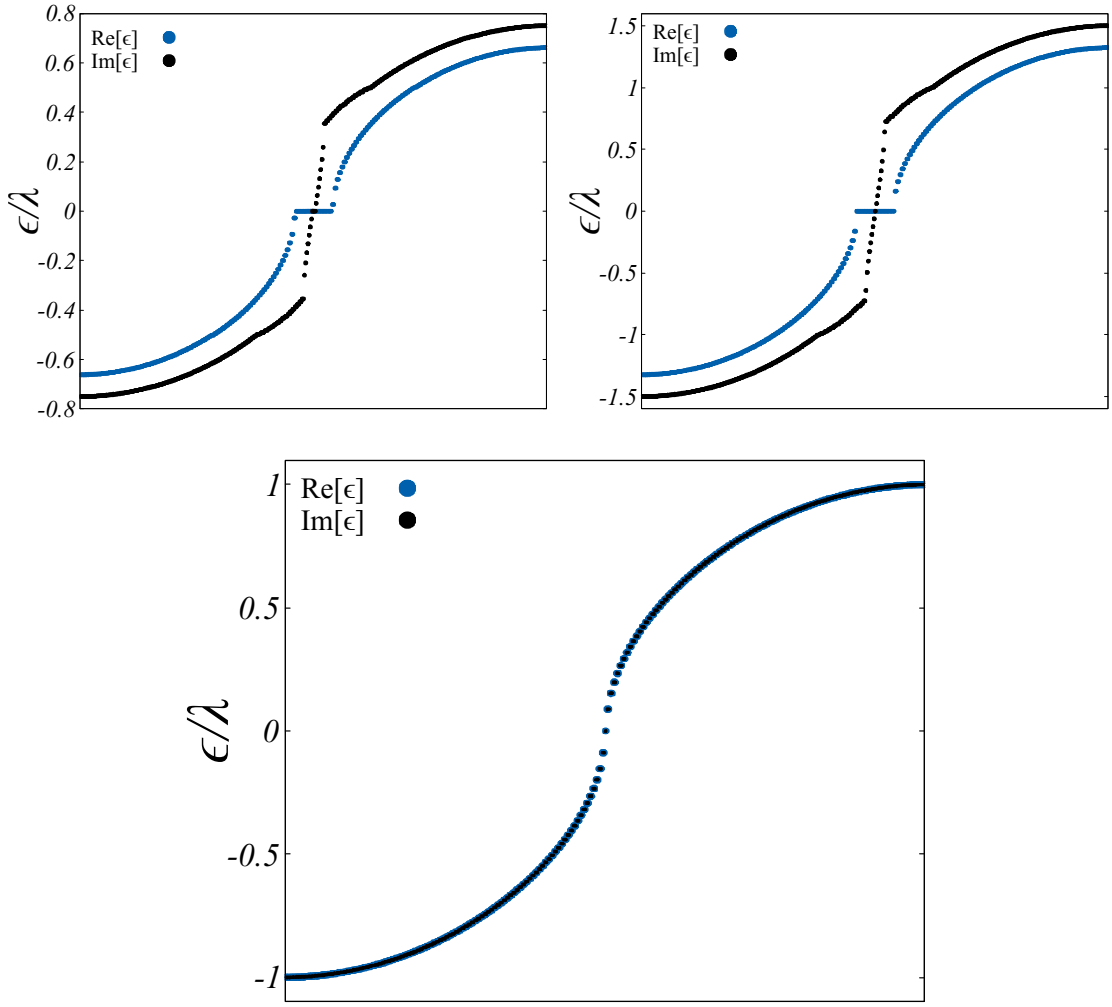

Figure 3.14: Eigenvalues for a 401 sites chain with even symmetry for the case with $\alpha_1 = -\beta_2 = 1/2$ and $\alpha_2 = -\beta_1 = 1$ (on the left) and for the case with $\alpha_1 = -\beta_2 = 1$ and $\alpha_2 = -\beta_1 = 1$. In both images, the real part is showed in blue and the imaginary part is in black.

Chapter 4

Conclusions

As we already discussed in chapter 1, it is possible to work with optical structures, photonic crystals, as we would do with ionic lattices in solid-state physics (crystals). We can find similar structures from Maxwell's equations and the Schrödinger equation, being both differential equations, which allows us to do that. We also noticed that the specific formalism used by us in this work shows useful features, as the possibility to avoid accidental degeneracies that could emerge using the usual formalism for photonic crystals.

With a more detailed overview of what are and how o describe photonic crystals, it is possible to see that the topological discussion, presented in chapter 2, can be extended to those systems. Therefore, we can use topological invariants to study topological phase transitions in photonic crystals. Even though the Zak phase shows different properties than the Berry phase, it is a useful topological invariant due to the shift $|\gamma_n| = \pi$ for a phase transition. This phase transition can be generated by closing and reopening a gap as we perform the adiabatic evolution of the system's Hamiltonian in k-space.

For the studied model, which is the most simple one-dimensional photonic crystal with interesting topological properties, it is possible to see the change in the Zak phase's value. This change of $|\pi|$, around the critical point, is connected to the appearance of topological end modes. Even though the Zak phase's gauge dependence can give misleading information, as we have discussed in chapter 3, this phase shift is sufficient to recognize the phase transitions.

The results for the model show that it is possible to make analogies for photonic crystals, compared to regular topological insulators. The edge states are robust under adiabatic evolution of the system as for random impurities on it. As we are working with classical light, it is necessary to keep in mind that the edge states are no localized photons but a sign of a higher intensity of the electromagnetic field within the specific site on the *lattice*. Changing the external conditions (next to the ends of the photonic system, as proposed in [27]) should be a useful solution to observe this experimentally.

The fact that we can see the topological phase transitions in photonic crystals, in an analogous way to the quantum lattices, turns out to be a helpful experimental advantage. It is easier to build a photonic topological insulator rather than a quantum topological insulator. Thus, the possibility to use these analogies between photonic systems and solid-state systems presents an experimental advantage. It is possible to look for topological manifestations in photonic crystals before the quantum realization. On the other hand, photonic topological insulators might be useful on their own, as the applications for these devices go from telecommunication technology, filters, or even detectors or other technological devices.

Future Work

For future work, the first interesting question is to understand if there is a physical interpretation of the Zak phase in photonic crystals. We know there is a relation between the Zak phase and the electric polarization, in a regular crystal. But for photonic crystals, we have no clarity about an interpretation. It would also be interesting to get further into metamaterials. We could question if it is possible to build a topological metamaterial insulator and a general form to calculate the Zak phase, including a general physical interpretation.

Appendix A

Adiabatic Theorem

The time-dependant Schrödinger equation is, in a general form,

$$\hat{H}(t)\left|\Psi(t)\right\rangle = i\frac{d}{dt}\left|\Psi(t)\right\rangle. \tag{A.1}$$

Assuming that the system at $t = 0$ is in the nth eigenstate, $|\psi_n\rangle$, it is possible to expand the wave function in terms of an orthonormal basis. This is,

$$\left|\Psi(t)\right\rangle = \sum_n c_n(t) e^{-\frac{i}{\hbar}\int_0^t E_n(t')dt'}\left|\psi_n(t)\right\rangle, \tag{A.2}$$

where $|\psi_n(t)\rangle$ is an eigenstate of $\hat{H}(t)$ with eigenvalue $E_n(t)$, the exponent $-\frac{1}{\hbar}\int_0^t E_n(t')dt'$ is the dynamic phase factor, and it satisfies

$$\langle\psi_n(t)|\psi_m(t')\rangle = \delta_{nm}\delta(t-t'). \tag{A.3}$$

Using this expansion for the wave function into the right side of the time-dependant Schrödinger equation, we get

$$\begin{aligned} i\hbar\frac{\partial}{\partial t}\left|\Psi(t)\right\rangle &= i\hbar\frac{\partial}{\partial t}\sum_n c_n(t) e^{-\frac{i}{\hbar}\int_0^t E_n(t')dt'}\left|\psi_n(t)\right\rangle \\ = i\hbar\sum_n &\left(\dot{c}_n(t)\left|\psi_n(t)\right\rangle + c_n(t)\left|\dot{\psi}_n(t)\right\rangle - \frac{i}{\hbar}E_n(t)c_n(t)\left|\psi_n(t)\right\rangle\right), \end{aligned} \tag{A.4}$$

and for the left side, we get

$$\begin{aligned}\hat{H}(t)\left|\Psi(t)\right\rangle &= \hat{H}(t)\sum_n c_n(t)e^{-\frac{i}{\hbar}\int_0^t E_n(t')dt'}\left|\psi_n(t)\right\rangle \\ &= \sum_n c_n(t)e^{-\frac{i}{\hbar}\int_0^t E_n(t')dt'}\hat{H}(t)\left|\psi_n(t)\right\rangle \\ &= \sum_n c_n(t)e^{-\frac{i}{\hbar}\int_0^t E_n(t')dt'}E_n(t)\left|\psi_n(t)\right\rangle . \end{aligned} \tag{A.5}$$

Then, comparing both sides of the equation, we obtain that

$$\boxed{\sum_n \dot{c}_n(t)e^{-\frac{i}{\hbar}\int_0^t E_n(t')dt'}\left|\psi_n(t)\right\rangle = -\sum_n c_n(t)e^{-\frac{i}{\hbar}\int_0^t E_n(t')dt'}\left|\dot{\psi}_n(t)\right\rangle .} \tag{A.6}$$

Now we calculate the inner product using the wave function $\langle\psi_{n'}(t)|$ and obtain

$$\dot{c}_{n'}(t) = -\sum_n c_n(t)e^{-\frac{i}{\hbar}\int_0^t (E_n(t')-E_{n'}(t'))dt'}\left\langle\psi_{n'}(t)|\dot{\psi}_n(t)\right\rangle . \tag{A.7}$$

Differentiating Equation A.1 we can get an expression for $\langle\psi_{n'}(t)|\dot{\psi}_n(t)\rangle$. Then,

$$\dot{c}_{n'}(t) = -c_{n'}(t)\left\langle\psi_{n'}(t)|\dot{\psi}_{n'}(t)\right\rangle - \sum_{n\neq n'} c_n(t)\frac{\left\langle\psi_{n'}(t)\right|\dot{\hat{H}}(t)\left|\psi_n(t)\right\rangle}{E_n(t)-E_{n'}(t)}e^{-\frac{i}{\hbar}\int_0^t (E_n(t')-E_{n'}(t'))dt'}. \tag{A.8}$$

As we are evolving the system adiabatically, the term with $\dot{\hat{H}}(t)$ is small, thus we get

$$\dot{c}_{n'}(t) \approx -c_{n'}(t)\left\langle\psi_{n'}(t)|\dot{\psi}_{n'}(t)\right\rangle , \tag{A.9}$$

and the solution for this differential equation is

$$c_n(t) = c_n(0)\exp\left(\underbrace{-\int_0^t \left\langle\psi_n(t')|\dot{\psi}_n(t')\right\rangle dt'}_{i\gamma_n(t)}\right), \tag{A.10}$$

with

$$\gamma_n(t) = i\int_0^t \left\langle\psi_n(t')|\dot{\psi}_n(t')\right\rangle dt'. \tag{A.11}$$

Appendix B

Berry Phase's gauge independence

The Berry phase is defined as

$$\gamma_n(\mathcal{C}) = i \oint_{\mathcal{C}} \langle n(\mathbf{R}(t))|\nabla_{\mathbf{R}} n(\mathbf{R}(t))\rangle \, d\mathbf{R}. \tag{B.1}$$

For $|\tilde{n}(\mathbf{R}(t))\rangle = \exp(i\phi(\mathbf{R}(t)))\,|n(\mathbf{R}(t))\rangle$ the Berry phase would be

$$\begin{aligned}
\tilde{\gamma}_n(\mathcal{C}) &= i \oint_{\mathcal{C}} \langle \tilde{n}(\mathbf{R}(t))|\nabla_{\mathbf{R}} \tilde{n}(\mathbf{R}(t))\rangle \, d\mathbf{R}, && \text{(B.2)}\\
&= i \oint_{\mathcal{C}} \langle n(\mathbf{R}(t))|\, e^{-i\phi(\mathbf{R}(t))}\nabla_{\mathbf{R}} \left(e^{i\phi(\mathbf{R}(t))}\,|n(\mathbf{R}(t))\rangle \right) d\mathbf{R}, && \text{(B.3)}\\
&= i \oint_{\mathcal{C}} \left[\langle n(\mathbf{R}(t))|\nabla_{\mathbf{R}} n(\mathbf{R}(t))\rangle + i\,\langle n(\mathbf{R}(t))|\,\nabla_{\mathbf{R}}\phi(\mathbf{R}(t))\,|n(\mathbf{R}(t))\rangle\right] d\mathbf{R}, && \text{(B.4)}\\
&= \gamma_n(\mathcal{C}) - \oint \nabla_{\mathbf{R}}\phi(\mathbf{R}(t)) d\mathbf{R}, && \text{(B.5)}\\
&= \gamma_n(\mathcal{C}) - \phi(\mathbf{R}(t))\Big|_0^T, && \text{(B.6)}\\
&= \gamma_n(\mathcal{C}) - 2\pi m, && \text{(B.7)}
\end{aligned}$$

and as m is an integer even though γ_n can be not the same as $\tilde{\gamma}_n$, the phase factor $e^{i\gamma_n}$ and $e^{i\tilde{\gamma}_n}$ have the same value.

Appendix C

The Honeycomb Lattice: Symmetries and Spectrum

As we mentioned in subsection 2.5.2, graphene is a two-dimensional material, conformed by carbon atoms in a honeycomb lattice. In this appendix, we intend to give a more detailed discussion about some of the symmetrical features of graphene, as they are related to the interesting topological features of it. To define the honeycomb lattice, we use the lattice vectors $\mathbf{R}_1 = \frac{a}{2}(3, \sqrt{3})$ and $\mathbf{R}_2 = \frac{a}{2}(3, -\sqrt{3})$. It is possible to use these two vectors to define a rhombus, which is a unit cell, as in C.1.

One of the most notorious symmetries of the hexagon is the C_6 symmetry, which takes a vertex into the next one. Straightforwardly, it has also C_3 and C_2 symmetries as $C_3 = C_6^2$ and $C_2 = C_6^3$. The other symmetries present are mirror symmetries, as m_y and m_x. However, for the mirror symmetries, if we consider only the generators, one of them would is sufficient.

Let us check how some of these symmetries operation acts on the lattice vectors.

$$
\begin{aligned}
C_3: &\quad \vec{R}_1 \to -\vec{R}_2, \quad \vec{R}_2 \to \vec{R}_1 - \vec{R}_2 \\
C_2: &\quad \vec{R}_1 \to -\vec{R}_1, \quad \vec{R}_2 \to -\vec{R}_2 \\
m_y: &\quad \vec{R}_1 \to \vec{R}_2, \quad \vec{R}_2 \to \vec{R}_1
\end{aligned}
$$

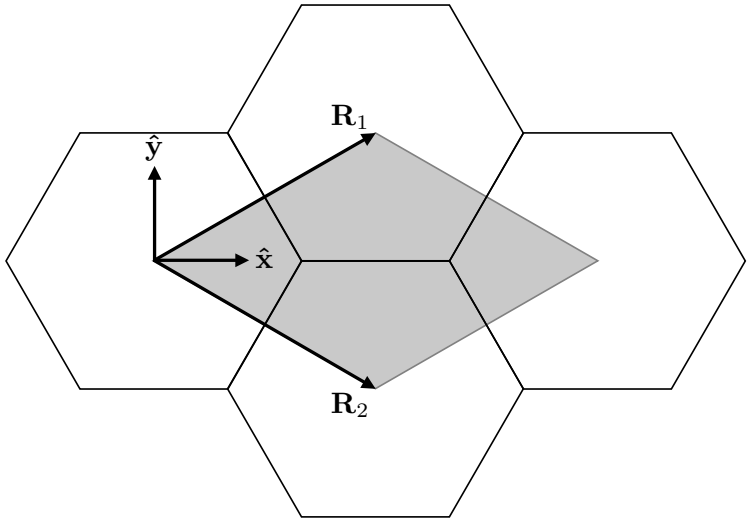

Figure C.1: An hexagonal lattice described by vectors $\mathbf{R}_1$ and $\mathbf{R}_2$. The gray rhombus is a unit cell.

The reason why we do not look at the C_6 symmetry operation will be clarified later.

Now the question is, 'what if we put atoms at positions q within the unit cell?" These positions are known as Wyckoff positions [28]. Then, if we put an atom at a given q, there will also be atoms at gq, where g is an element of the space symmetry group $\mathcal{G}$, which is $p6m$ in this case. We call the orbit of q as all the elements $q = \{gq; g \in \mathcal{G}\}$. Now, we can look for the *Stabilizer group of* q, $\mathcal{G}_q = \{g \in \mathcal{G}_q; gq = q\}$, which is the group of all the elements g which let the point q invariant. For a random point q' within the hexagon, not on a special symmetrical point, the stabilizer group of q' would be the identity $\{E\}$. The stabilizer group is isomorphic to the point group.

Now we look for special Wyckoff positions, using $a = \dfrac{1}{\sqrt{3}}$, for simplicity. We are going to look 4 special positions, q^{3c}, q^{2b}, q^{1a} and q^x (this last position is not going to be much relevant for the purpose of this appendix), which are depicted in Figure C.1.

Let us define $q^{3c} = \dfrac{\vec{R}_1 - \vec{R}_2}{2}$, then we have $\mathcal{G}_{q^{3c}} := \left\{\left\{C_2|\vec{R}_1 - \vec{R}_2\right\}, \{m_x\}\right\} \simeq C_{2v}$. Thus, the stabilizer group of the point q^{3c} is isomorphic to C_{2v}.

Then, we define $q^{2b} = \dfrac{\vec{R}_1 + \vec{R}_2}{3}$, and therefore $\mathcal{G}_{q^{2b}} := \{\{C_3|vecR_2\}, \{m_y\}\} \simeq C_{3v}$. Thus, the stabilizer group of the point q^{2b} is isomorphic to C_{3v}.

Now, we define $q^{1a} = \vec{0}$, whose stabilizer group is the whole group $\mathcal{G}_{q^{1a}} = \mathcal{G} := \{R|T_\mu\}$,

where R corresponds to the beforementioned rotations and T_μ to translations in $\vec{R}_1$ and $\vec{R}_2$.

Finally, we have q^x, which is $q^x := x\left(\vec{R}_1 + \vec{R}_2\right)$, $x \in \left(0, \frac{1}{3}\right)$. Then, the stabilizer group of q^x is $\mathcal{G}_{q^x} := \{\{m_y\}\}$.

Now we can look for the orbit of the given Wyckoff positions. The objective behind this is to characterize the special positions where we can put atoms.

For q^{3c}, if we apply C_3, which is in the symmetry group but no in the stabilizer group, we obtain another site and the same with ${C_3}^2$. Therefore, we have three sites in this Wyckoff position: q^{3c}, $C_3 q^{3c}$ and ${C_3}^2 q^{3c}$. Thus, this given Wyckoff position has a multiplicity of 3. For the last two points, we are considering translations T_{R_1} and T_{R_2} to leave them at the same unit cell, which is the same to take C_6^{-1} and C_6, respectively.

For q^{2b}, we apply C_2 and get two sites in this Wyckoff position: q^{2b} and $C_2 q^{2b}$. Therefore, this Wyckoff position is of multiplicity 2.

For q^{1a}, its orbit is the full symmetry group, as all the elements in it leave it invariant. It is a Wyckoff position of multiplicity 1.

For the specific case of graphene, carbon atoms are located at position q^{2b}. Now, as we are interested in graphene, we would like to address that q^{2b} is a maximal Wyckoff position. There are no subgroups between the site symmetry group of q^{2b}, $\mathcal{G}_{q^{2b}}$, and the full space symmetry group $\mathcal{G}$.

As we now know about the symmetries of the previously discussed positions, it is possible to use other group theory tools to analyze the system's band structure if we put orbitals in these sites. However, for this appendix's purpose, the information about the spatial symmetries of the discussed points are the needed information.

The analysis of the symmetries of positions q^{1a}, q^{2b} and q^{3c}, was considering the idea to put orbitals in the real space lattice. However, as we know, the reciprocal lattice of the honeycomb lattice is also a honeycomb lattice. Therefore, the reciprocal lattice has the same symmetrical points as the real space one. These points are known as high symmetry points and are designated with letters Γ, for $k = 0$, which has the same symmetries as the point q^{1a}. K, (or K') for the vertex of the hexagon, similar to q^{2b}. M for the point between two vertices, as the point q^{3c}.

The reason why K and K' are used is due to both points are related, spatially, by C_2 symmetry but are no equivalent up to translations. If we were going to label the six hexagon's vertices on the reciprocal space, three of them would be labeled as K, and the other three would be labeled as K'. In the first Brillouin zone there are only one K and one K'. Why are these two points interesting? The answer is that these two points are related by inversion symmetry and time-reversal symmetry.

Inversion symmetry is such that turns $(x, y) \rightarrow (-x, -y)$ and time-reversal symmetry turns $\mathbf{k} \rightarrow -\mathbf{k}$. Considering what we have already discussed about the geometrical symmetries of the hexagonal lattice it is easy to see the connection between these two points.

We know that a Hamiltonian is symmetric under time-reversal symmetry if it fulfills the condition $\mathcal{T}H(\mathbf{k})\mathcal{T}^{-1} = H(-\mathbf{k}) = H^*(\mathbf{k})$ and is symmetric under inversion symmetry if $\mathcal{I}H(\mathbf{k})\mathcal{I}^{-1} = \pm H(\mathbf{k})$, where the sign depends on the parity, even or odd. For the spinless graphene's case, both of these symmetries, together, lead to the fact that there are no gaps at the special points K and K'. Therefore, to open a gap, it is necessary to break these symmetries.

Appendix D

The Corbino Geometry and the Laughlin Pump

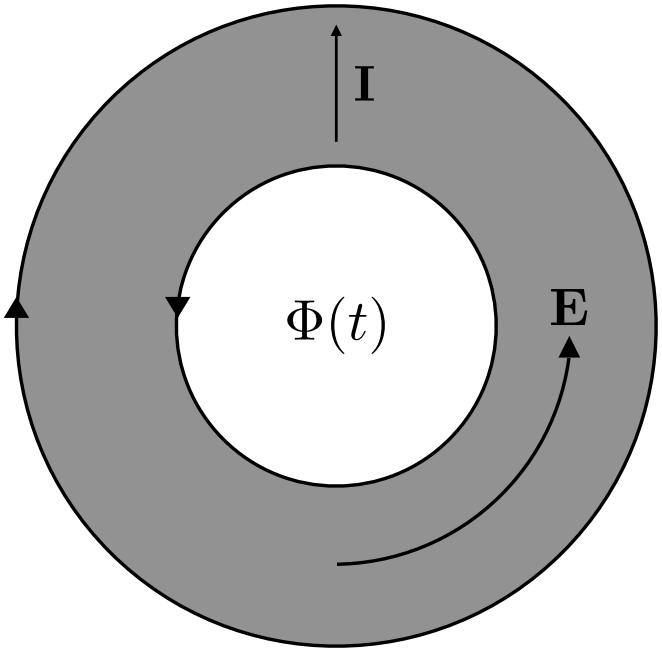

Figure D.1: Schematic representation of the Corbino disk.

Let us consider the Hall problem in an annular geometry, known as the Corbino disk [5, 29], as show in Figure D.1. In this case, the main idea is to measure the charge transfer, ΔQ, between the edges, in the presence of a tangential electric field. It is possible to gen-

erate that electric field by turning on a time-dependent magnetic flux. Then, considering Faraday's law, $|\oint d\mathbf{r}\cdot\mathbf{E}| = |\partial_t\Phi(t)|$, and assuming that $\mathbf{E}$ depends only on the radius R, the tangential electric field is

$$E(R,t) = \frac{1}{2\pi R}\partial_t\Phi(t). \tag{D.1}$$

From Ohm's law, we know that $\mathbf{J} = \sigma\mathbf{E}$, and in this case, we have $I = J\cdot 2\pi R$. Therefore, the Hall conductivity is

$$\sigma_H = \frac{I}{\partial_t\Phi(t)}. \tag{D.2}$$

We are assuming that the longitudinal conductivity vanishes, as seen experimentally.

Then, if we change the magnetic flux by $\Delta\Phi = \frac{h}{e}$ over time Δt, the transferred charge, $\Delta Q = I\Delta t$, between the edges is given by

$$\begin{aligned} \Delta Q &= \sigma_H\partial_t\Phi(t)\Delta t \\ &= \sigma_H\Delta\Phi(t) \\ &= \sigma_H\frac{h}{e} \\ \Rightarrow \sigma_H &= \Delta Q\frac{e}{h}, \end{aligned} \tag{D.3}$$

and ΔQ should be an integer number of electrons.

Let us take a "Hall cylinder", which is made by wrapping a 2D Hall sample in such a way that its ends are attached together. The cylinder is as the one shown in Figure D.2. The x coordinate is now curved and lives in the mantle of the cylinder.

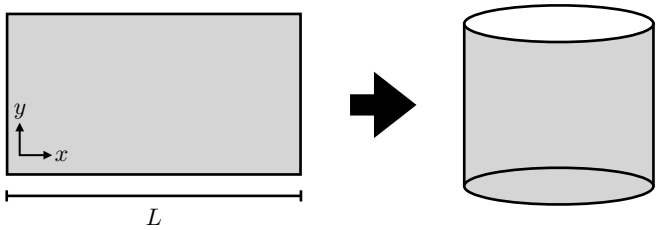

Figure D.2: Construction of a Hall cylinder

If we consider a cylinder with a magnetic flux Φ through its axis we will have, from Ohm's law,

$$\sigma_H = \frac{I}{\partial_t \Phi}, \tag{D.4}$$

where $I = \Delta Q/\Delta t$. Therefore,

$$\Delta Q = \sigma_H \Delta t \partial_t \Phi \tag{D.5}$$

$$\Delta Q = \sigma_H \Delta \Phi. \tag{D.6}$$

If we set the **change in the flux**, $\Delta\Phi$, to be h/e, then the charge variation will be $\Delta Q = ne$, as we expected.

Another feature that we should look out about the QHE is the energy of the transported electrons. As there is an applied magnetic field, their momentum is transformed as $\mathbf{p} \to \mathbf{p} - \frac{e}{c}\mathbf{A}$ and, their energy will be quantized in Landau levels, with their corresponding wavefunctions, centered at a certain point which will move from n to $n-1$, with each change in the magnetic flux by h/e. This is because every time we increase the flux in h/e, a Landau level crosses the Fermi level and, therefore, another Landau level is filled.

The potential, which defines the Hall cylinder, has to be sharp at the edges to be able to confine the electrons within it. However, it does not define a current between the edges. Both edges are separated by the bulk, which can not carry a current due to the position of the Fermi level. The chiral states, near to the edges, have a dispersion of the form

$$E(\mathbf{k}) = \hbar v(\mathbf{k} - \mathbf{k}_F), \tag{D.7}$$

where $\mathbf{k}_F$, the Fermi momentum, is $\mathbf{k}_F = 2\pi N\hat{x}/L$, with N the number of electrons and L the length of the sample or the cylinder's perimeter in this case.

As we know, in the presence of an applied magnetic field, the electrons will describe cyclotron orbits. However, the electrons near the edges will not be able to complete an orbit, and, as they can not escape, they will bounce back inside it within the sample and will describe **skipping orbits**, moving through the edges. These electrons, defined as **chiral states**, move with a velocity given by $v = E_y/B$, where $E_y = \partial_y V(y)$. It is

important to clarify that the electrons at different edges will move opposite in direction. A simple, schematic, representation of this is depicted in Figure D.3.

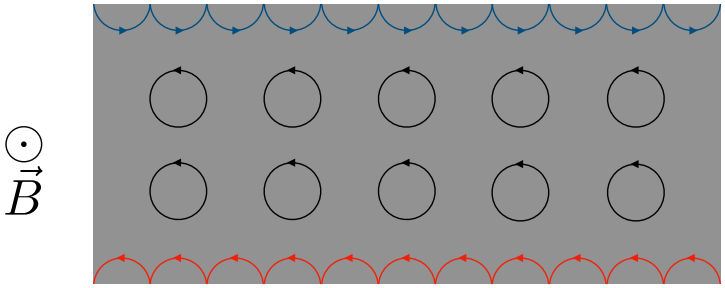

Figure D.3: Schematic illustration of the chiral states, and the other states, on a Hall Cylinder's portion.

It is possible to obtain a value for the Hall conductance from the existence of these chiral states. As there is the same number of electrons going to one direction as for the other, at each edge, the net current is zero. However, if there is a small voltage difference between these edges, there will be a different number of electrons at each edge. Therefore, in this case, the total current will be non-zero and is given by $I = \sigma_H V$. As the electrons can not backscatter, they have the highest possible conductance, which is $G = e^2/h$. Finally, for every chiral state, we will have a transport channel for the current. Therefore, the net current will be

$$I = n\frac{e^2}{h}V, \tag{D.8}$$

where n is the number of channels, or chiral states. As we can see, the value for the Hall conductance that we obtained via the analysis of the chiral states is the same that we obtained using the Nakano-Kubo formula, which leads to the first Chern number calculation.

Appendix E

Zak phase Quantization

The Zak phase is

$$\begin{aligned} \gamma_n &= i \int_{\mathbf{BZ}} \langle u_{nk} | \, \partial_k \, | u_{nk} \rangle \, dk \\ &= i \int_{\mathbf{BZ}} \int_{\Omega} u^*_{nk}(x) \partial_k u_{nk}(x) dx dk \end{aligned} \tag{E.1}$$

where $u_{nk}(x) = e^{ikx}\psi_{nk}(x)$ is the periodic part of the Bloch function, **BZ** is the first Brillouin zone and Ω is the unit cell length (a).

It's possible to rewrite the Bloch function in terms of the Wannier functions, this is

$$\psi_{nk}(x) = \sum_m e^{ikma} a_n(x - ma), \tag{E.2}$$

then, we can get $u_{nk}(x)$ in terms of the Wannier functions,

$$u_{nk}(x) = \sum_m e^{-ik(x-ma)} a_n(x - ma). \tag{E.3}$$

Then the Zak phase is equals to,

$$\begin{aligned}
\gamma_n &= \int_{\mathbf{BZ}} \sum_{m,m'} e^{-ik(m-m')a} \int_\Omega a_n^*(x-ma)(x-m'a)a_n(x-m'a)dxdk \\
&= \frac{2\pi}{a} \sum_{m,-m'} \delta_{m,m'} \int_\Omega a_n^*(x-ma)(x-m'a)a_n(x-m'a)dx \\
&= \frac{2\pi}{a} \sum_m \int_0^a a_n^*(x-ma)(x-ma)a_n(x-ma)dx \\
&= \frac{2\pi}{a} \int_{-\infty}^{\infty} x'|a_n(x')|^2 dx'. \qquad \text{(E.4)}
\end{aligned}$$

If the system is symmetric (or antisymmetric) under inversion, then the integral in x could only take the values 0 or $\frac{a}{2}$. Then, the Zak phase is 0 or π.

Appendix F

The Inner Product Redefinition

An operator constructed as the product of two Hermitian operators, such as $M = WD$ is non-Hermitian if $[W, D] \neq 0$. However, it's possible to redefine the inner product in order to get $\langle\varphi|\, M\, |\psi\rangle = \langle\psi|\, M^\dagger\, |\varphi\rangle^*$.

$$\begin{aligned}
\langle\varphi|\, M\, |\psi\rangle_W &= \langle\varphi|\, W^{-1}M\, |\psi\rangle \\
&= \langle\varphi|\, W^{-1}WD\, |\psi\rangle \\
&= \langle\varphi|\, D\, |\psi\rangle \\
&= \langle\psi|\, D\, |\varphi\rangle^* \\
&= \langle\psi|\, DWW^{-1}\, |\varphi\rangle^* \\
&= \langle\psi|\, M^\dagger W^{-1}\, |\varphi\rangle^* \\
&= \langle\psi|\, M^\dagger\, |\varphi\rangle^*_W\,. \qquad \text{(F.1)}
\end{aligned}$$

Appendix G

The Real Space Hamiltonian

We take the Hamiltonian of our system, defined in chapter 3,

$$\mathcal{H}(k) = \begin{pmatrix} 0 & 0 & -i\alpha_1 & i\alpha_1 e^{ika} \\ 0 & 0 & i\beta_1 & -i\beta_1 \\ i\alpha_2 & -i\alpha_2 & 0 & 0 \\ -i\beta_2 e^{-ika} & i\beta_2 & 0 & 0 \end{pmatrix}, \tag{G.1}$$

and perform the expansion (2.62),

$$\begin{aligned} \hat{H} &= \frac{1}{N}\sum_k \sum_{n,n'} e^{ika(n-n')} (a_n^\dagger, b_n^\dagger, c_n^\dagger, d_n^\dagger) \begin{pmatrix} 0 & 0 & -i\alpha_1 & i\alpha_1 e^{ika} \\ 0 & 0 & i\beta_1 & -i\beta_1 \\ i\alpha_2 & -i\alpha_2 & 0 & 0 \\ -i\beta_2 e^{-ika} & i\beta_2 & 0 & 0 \end{pmatrix} \begin{pmatrix} a_{n'} \\ b_{n'} \\ c_{n'} \\ d_{n'} \end{pmatrix}, \\ &= \frac{1}{N}\sum_k \sum_{n,n'} e^{ika(n-n')} \Big[i\alpha_1 \left(e^{ika} a_n^\dagger d_{n'} - a_n^\dagger c_{n'} \right) + i\beta_1 \left(b_n^\dagger c_{n'} - b_n^\dagger a_{n'} \right) \\ &\qquad -i\alpha_2 \left(c_n^\dagger b_{n'} - c_n^\dagger a_{n'} \right) - i\beta_2 \left(d_n^\dagger b_{n'} - e^{-ika} d_n^\dagger a_{n'} \right) \Big], \\ &= \frac{1}{N}\sum_{n,n'} \Big[i\alpha_1 \left(\delta_{n,n'-1} a_n^\dagger d_{n'} - a_n^\dagger c_{n'} \right) + i\beta_1 \left(b_n^\dagger c_{n'} - b_n^\dagger a_{n'} \right) \\ &\qquad -i\alpha_2 \left(c_n^\dagger b_{n'} - c_n^\dagger a_{n'} \right) - i\beta_2 \left(d_n^\dagger b_{n'} - \delta_{n,n'+1} d_n^\dagger a_{n'} \right) \Big]. \end{aligned} \tag{G.2}$$

Bibliography

[1] C. Nash and S. Sen. *Topology and Geometry for Physicists*. Dover, Mineola, NY, 2011.

[2] Michael Victor Berry. Quantal phase factors accompanying adiabatic changes. *roceedings of the Royal Society of London. A.*, 392:45–57, Mar 1984.

[3] Di Xiao, Ming-Che Chang, and Qian Niu. Berry phase effects on electronic properties. *Rev. Mod. Phys.*, 82:1959–2007, Jul 2010.

[4] E. Kaxiras. *Atomic and Electronic Structure of Solids*. Cambridge University Press, New York, NY, 2003.

[5] R. B. Laughlin. Quantized hall conductivity in two dimensions. *Phys. Rev. B*, 23:5632–5633, May 1981.

[6] F. D. M. Haldane. Model for a quantum hall effect without landau levels: Condensed-matter realization of the "parity anomaly". *Phys. Rev. Lett.*, 61:2015–2018, Oct 1988.

[7] W. P. Su, J. R. Schrieffer, and A. J. Heeger. Solitons in polyacetylene. *Phys. Rev. Lett.*, 42:1698–1701, Jun 1979.

[8] P. Delplace, D. Ullmo, and G. Montambaux. Zak phase and the existence of edge states in graphene. *Phys. Rev. B*, 84:195452, Nov 2011.

[9] C. L. Kane and E. J. Mele. Quantum spin hall effect in graphene. *Phys. Rev. Lett.*, 95:226801, Nov 2005.

[10] C. L. Kane and E. J. Mele. Z_2 topological order and the quantum spin hall effect. *Phys. Rev. Lett.*, 95:146802, Sep 2005.

[11] B. Andrei Bernevig and Taylor L. Hughes. *Topological Insulators and Topological Superconductors*. Princeton University Press, Princeton, NJ, 2013.

[12] J. Zak. Berry's phase for energy bands in solids. *Phys. Rev. Lett.*, 62:2747–2750, Jun 1989.

[13] Nicola Marzari, Arash A. Mostofi, Jonathan R. Yates, Ivo Souza, and David Vanderbilt. Maximally localized wannier functions: Theory and applications. *Rev. Mod. Phys.*, 84:1419–1475, Oct 2012.

[14] Marcos Atala, Monika Aidelsburger, Julio T. Barreiro, Dmitry Abanin, Takuya Kitagawa, Eugene Demler, and Immanuel Bloch. Direct measurement of the zak phase in topological bloch bands. *Nature Physics*, 9:795, Nov 2013.

[15] John D. Joannopoulos, Steven G. Johnson, J. N. Winn, and R. D. Meade. *Photonic Crystals*. Princeton University Press, Princeton, NJ, 2008.

[16] M. Skorogogatiy and J. Yang. *Fundamentals of Photonic Crystal Guiding*. Cambridge University Press, New York, NY, 2009.

[17] Mikael C. Rechtsman, Yonatan Plotnik, Julia M. Zeuner, Daohong Song, Zhigang Chen, Alexander Szameit, and Mordechai Segev. Topological creation and destruction of edge states in photonic graphene. *Phys. Rev. Lett.*, 111:103901, Sep 2013.

[18] S. Raghu and F. D. M. Haldane. Analogs of quantum-hall-effect edge states in photonic crystals. *Phys. Rev. A*, 78:033834, Sep 2008.

[19] J. D. Jackson. *Classical Electrodynamics*. John Wiley & Sons, Inc., Hoboken, NJ, 1999.

[20] Giuseppe De Nittis and Max Lein. Derivation of ray optics equations in photonic crystals via a semiclassical limit. *Annales Henri Poincaré*, 18(5):1789–1831, May 2017.

[21] Giuseppe De Nittis and Max Lein. The schrödinger formalism of electromagnetism and other classical waves—how to make quantum-wave analogies rigorous. *Annals of Physics*, 396:579 – 617, 2018.

[22] N. Moiseyev. *Non-Hermitian Quantum Mechanics*. Cambridge University Press, Cambridge, United Kingdom, 2011.

[23] Alexei Kitaev. Periodic table for topological insulators and superconductors. *AIP Conference Proceedings*, 1134(1):22–30, 2009.

[24] Ching-Kai Chiu, Jeffrey C. Y. Teo, Andreas P. Schnyder, and Shinsei Ryu. Classification of topological quantum matter with symmetries. *Rev. Mod. Phys.*, 88:035005, Aug 2016.

[25] Jun-Won Rhim, Jan Behrends, and Jens H. Bardarson. Bulk-boundary correspondence from the intercellular zak phase. *Phys. Rev. B*, 95:035421, Jan 2017.

[26] R. D. King-Smith and David Vanderbilt. Theory of polarization of crystalline solids. *Phys. Rev. B*, 47:1651–1654, Jan 1993.

[27] Ka Hei Choi, C. W. Ling, K. F. Lee, Y. H. Tsang, and Kin Hung Fung. Simultaneous multi-frequency topological edge modes between one-dimensional photonic crystals. *Opt. Lett.*, 41(7):1644–1647, Apr 2016.

[28] L. Kantorovich. *Quantum Theory of the Solid State: An Introduction*. Springer Netherlands, Dordrecht, NL, 2004.

[29] DelftX. Where do the pumped electrons come from and go to? - Topology in Condensed Matter, 2014", howpublished = "`https://topocondmat.org/w3_pump_QHE/QHEedgestates.html`", note = "[Online; accessed 19-November-2018]".